NASA Technical Paper 1199

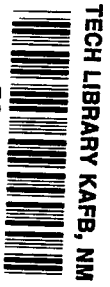

Simulated Flight Effects on Noise Characteristics of a Fan Inlet With High Throat Mach Number

Howard L. Wesoky, Donald A. Dietrich,
and John M. Abbott

APRIL 1978

NASA

NASA Technical Paper 1199

Simulated Flight Effects on Noise Characteristics of a Fan Inlet With High Throat Mach Number

Howard L. Wesoky, Donald A. Dietrich,
and John M. Abbott
Lewis Research Center
Cleveland, Ohio

National Aeronautics
and Space Administration

**Scientific and Technical
Information Office**

1978

SIMULATED FLIGHT EFFECTS ON NOISE CHARACTERISTICS OF A FAN INLET WITH HIGH THROAT MACH NUMBER

by Howard L. Wesoky, Donald A. Dietrich, and John M. Abbott

Lewis Research Center

SUMMARY

An anechoic wind tunnel experiment was conducted to determine the effects of simulated flight on the noise characteristics of a high-throat-Mach-number (about 0.8) fan inlet. Comparisons were made with the performance of a conventional low-throat-Mach-number (about 0.6) inlet with the same 50.8-centimeter (20-in.) diameter fan noise source. Simulated forward velocity of 41 meters per second (80 knots) caused perceived noise level reductions of about 2 decibels for the low-throat-Mach-number inlet and more than 3 decibels for the high-throat-Mach-number inlet. High-throat-Mach-number-inlet perceived noise reduction capability, defined as the difference between the noise levels of the two inlets at the same fan operating condition, was as high as 7.5 decibels with tunnel airflow and about 6 decibels without tunnel airflow. Inlet pressure recovery was high and distortion low for flow angles up to 30^{o}, but the complex flow fields and generally small noise variations (about 2 dB for perceived noise) made the effects of inlet flow angle on noise seemingly irregular and difficult to characterize. Some modifications of tones at blade passage harmonics were noted. A low-throat-Mach-number-inlet lobed directivity pattern observed at nonzero flow angles for the second harmonic was effectively eliminated by the high-throat-Mach-number inlet. Also the tone at the blade passage frequency, which was cut off at zero inlet flow angle, was observed at nonzero inlet flow angles.

INTRODUCTION

As part of the Quiet Clean Short-Haul Experimental Engine (QCSEE) Project (ref. 1), a series of model experiments on installed performance have been conducted. In one of these experiments, a 50.8-centimeter (20-in.) diameter fan engine model was used to simulate engine inlet in-flight aerodynamic performance in the NASA Lewis Research Center 9- by 15-Foot V/STOL Wind Tunnel (ref. 2). The anechoic character of the wind

tunnel test section (refs. 3 and 4) also provided the opportunity to use the same fan engine model to obtain simulated flight-type acoustics data. Because this fan was not a model for the QCSEE propulsion systems, the acoustics data do not apply directly to the QCSEE Project. However, as indicated in earlier reports on this model fan (refs. 5 and 6), there is a scarcity of flight-type acoustics data obtained under well-controlled test conditions; and, therefore, the data from this experiment are significant as general technology.

This report examines data from the wind tunnel acoustics experiment that relate to the effect of flight on the noise reduction characteristic of a high-throat-Mach-number inlet. The high-throat-Mach-number (nearly choked flow) inlet concept of noise reduction has been well demonstrated and is the primary method of inlet noise control for the QCSEE propulsion systems. Previous wind tunnel experiments (refs. 7 and 8) have provided qualitative information about high-throat-Mach-number inlet aerodynamic and acoustic performance, but they have used sirens rather than a realistic fan noise source and were not conducted in an anechoic environment.

The model inlets of the current investigation were from a series of inlets examined by the General Electric Company for the QCSEE Project. Various inlet noise reduction techniques were investigated, including resonator acoustic treatment, bulk-absorber acoustic treatment, and a combination of nearly choked flow with acoustic treatment (i.e., a hybrid inlet). Static acoustic performance of all the inlets with a model QCSEE fan was obtained in an anechoic chamber and is reported in references 9 and 10. Simulated flight effects on the acoustic performance of treated inlets with conventional low throat Mach numbers are reported in reference 11 for the same fan noise source as the present report. Only the performance of inlets without acoustic treatment (i.e., "hard wall" inlets) is considered herein.

Baseline acoustic performance (i.e., without noise reduction) was determined for this report with a conventional inlet having a throat Mach number of about 0.6 at its design weight flow. At this weight flow, the corresponding throat Mach number for the other inlet, called the high-Mach inlet, was about 0.8. The amount of noise reduction attributable to the high-Mach inlet was determined by comparing its performance to the first inlet, called the low-Mach inlet, at the same fan operating condition.

Perceived noise levels and 1/3-octave-band sound pressure levels determined at tunnel airflow velocities of 0 and 41 meters per second (80 knots) and inlet flow angles up to 30° are presented. The model fan was operated over a range of rotational speeds to vary the inlet weight flow and to investigate noise reduction over a significant range of throat Mach number.

APPARATUS

Anechoic Wind Tunnel

Figure 1 is a schematic representation of the 8- by 6-Foot Wind Tunnel and the 9- by 15-Foot V/STOL Wind Tunnel at the NASA Lewis Research Center. Anechoic wind tunnel is the term used for the combination of the 2.7- by 4.6-meter (9- by 15-ft) low-speed test section, the tunnel drive motors, and the enclosed flow path. The low-speed test section is used for anechoic experimentation in the acoustic direct field within the test section during tunnel operation.

The test section has been used extensively for aerodynamic testing; its aerodynamic characteristics are reported in reference 12. That report indicates that the test section velocity profile is uniform and that the turbulence is low. The walls, floor, and ceiling of the test section are lined with acoustic treatment. Details of the treatment and the acoustic characteristics of the test section are reported in references 3 to 6. These reports state that anechoic or free-field properties exist for frequencies above 1000 hertz. For the purposes of acoustic testing, the anechoic wind tunnel has the favorable characteristics of remote drive motors, an acoustical muffler between the compressor and the test section, and acoustic treatment on the first turn upstream and the first turn downstream of the test section (fig. 1). With these features, the background noise level (1/3-octave band) in the test section is about 82 decibels at 1000 hertz for a 41-meter-per-second (80-knot) airflow velocity. The background noise level is lower at lower airflow velocities and at higher frequencies (ref. 4).

Model Fan

Model fan characteristics are given in table I. The 50.8-centimeter (20-in.) diameter model has 15 rotor blades, a design tip speed of 213 meters per second (700 ft/sec), and a rotor-to-stator spacing of 1 rotor chord. In the present study, the fan was operated to about 110 percent of the design speed. Although the rotor has variable-pitch capability, only the design blade angle is considered herein. Aerodynamic performance of the fan with 11 stator vanes, as originally designed, is reported in reference 13. According to reference 2, the aerodynamic performance of the 25-stator-vane configuration used in the present investigation is the same as that of the 11-vane configuration.

Consideration of the sound pressure level tones at harmonics of the blade passage frequency relative to center frequencies of 1/3-octave bands was used to help select the fan operating line (i.e., the nozzle area). Some of the acoustic design characteristics and tone cutoff properties of the fan are discussed in references 5 and 6. For this model, which has a stator-vane-to-rotor-blade ratio of 1.67, the theory of tone cutoff predicts

that the fundamental, or first, harmonic of the blade passage tone will not propagate below 107 percent of the design speed. However, according to reference 5, this theory does not consider any effect of the inlet radius contraction. According to the cutoff theory, the second harmonic tone will propagate at all fan rotational speeds. Propagation of the second harmonic is discussed in reference 6; it may be expected to exhibit a distinctively lobed directivity pattern when it is not masked by extraneous noise sources.

The fan was driven by an air turbine described in reference 14. Drive air was delivered to the turbine plenum through the vertical model support and pylon, as illustrated in figures 2 and 3, which show the general arrangement of the model in the wind tunnel test section. Fan and turbine discharge flows were ducted through a 90^{o} elbow to an acoustic muffler and exhausted outside the test section (ref. 2). An adjustable plug at the muffler exit (fig. 2(a)) allowed the remote setting of the exhaust nozzle area and thereby the fan operating point. The elbow and vertical duct were lined with acoustic treatment to suppress aft fan noise. In addition, turning vanes in the elbow were acoustically treated to prevent reflection of aft fan noise upstream. As shown in figure 2(b), the angle of the inlet to the tunnel airflow was varied by rotating the model in the horizontal plane.

Model Inlets

Model inlet characteristics are given in table II and figure 4. The inlets of the present experiment were part of a series of inlets built by the General Electric Company for the QCSEE Project and are further described in references 2 and 9. Baseline acoustic performance was defined in the present experiment with a conventional flight inlet having a low throat Mach number (about 0.6) at the inlet design condition. In further discussions, this inlet is called the low-Mach inlet. Noise reduction was examined with the other inlet (table II and fig. 4), which had a high throat Mach number (about 0.8) at the inlet design condition. This inlet is called the high-Mach inlet. The inlet design condition referred to in this report corresponds to that chosen for the QCSEE propulsion systems (refs. 1, 2, and 9) during aircraft takeoff operation. Except for the centerbody, the contour of the high-Mach inlet was the same as that chosen for the full-scale QCSEE propulsion systems.

An important characteristic of both inlets was the high internal-lip-area contraction ratio, 1.46, which allowed the inlets to sustain high angles to the free stream without flow separation, a required performance characteristic for short-takeoff-and-landing (STOL) aircraft operation. Both inlets provided little flow diffusion, with a ratio of fan annulus (diffuser exit) area to throat area of 1.011 for the low-Mach inlet and 1.156 for the high-Mach inlet. Without the centerbody, the ratios of diffuser exit area to throat area were 1.283 for the low-Mach inlet and 1.466 for the high-Mach inlet. Figure 4(b)

illustrates the difference in contours between the low- and high-Mach inlet cowls. Both inlets were axisymmetric and had length-to-fan-diameter ratios near 1.

INSTRUMENTATION

Acoustic

The primary acoustic instrumentation is shown in figure 3 and consisted of a "sword" microphone and a rotating microphone boom. A standard commercially available microphone head, 0.635 centimeter (0.250 in.) in diameter, with a bullet noise was used. The unique feature of the sword microphone system was the remote location of the cathode follower in the thickened portion of the vane support. This allowed a very thin streamlined microphone system that weathervaned above its support. Therefore, the microphone was always oriented directly into the airflow, which is the condition of minimum wind noise on the microphone.

The sword microphone was located 3.6 fan diameters from the intersection of the fan axis with the inlet highlight plane (fig. 2(b)). It was mounted on the end of a boom that rotated about a vertical axis through the inlet face (fig. 3). The microphone could be swept in a circular arc in the horizontal plane at the height of the fan axis.

Three other microphones, similar in design to the sword microphone but in fixed locations, were installed in the test section ceiling (fig. 3). The locations of these microphones were chosen to obtain data representative of a 152-meter (500-ft) ground sideline as an aircraft flew by at a 61-meter (200-ft) altitude in a takeoff configuration defined for the QCSEE Project (ref. 1). Details of this configuration are given in table III and will be further discussed with the results of the experiment. While these microphones were representative of aircraft sideline measurements, the arc defined by the sword microphone boom represented a flyover plane when tunnel flow was at an angle to the inlet axis.

Electrical signals from the microphones were conditioned in a conventional manner and recorded on magnetic tape. In addition, the signal from the sword microphone was processed with additional amplifiers, filters, and logarithmic converters to yield an on-line (real time) analysis of the acoustic signature. This system provided a plot of the inlet noise directivity pattern as the microphone boom was remotely rotated. Based on observation of measurement repeatability, the accuracy of acoustic measurements in this experiment is believed to have been about ±0.5 decibel of sound pressure level. However, reference 11 has indicated that, in at least one case, an inaccuracy of as much as 2 decibels occurred, which may be a better gage of the measurement uncertainty. This is discussed further with the results.

Aerodynamic

Aerodynamic instrumentation is completely defined and discussed in reference 2. Sixty-four static pressure taps were installed in the cowl walls of each inlet, with most of these in two rows at circumferential locations ψ of 0° and 200° (fig. 4). At a measuring plane indicated in figure 4(a), six rakes with 114 total pressure sensors were used to measure fan inlet pressure recovery and distortion. These rakes were, of course, removed for acoustic measurements.

At the fan stator exit, five rakes with 30 total pressure sensors and 5 total temperature sensors were used along with 10 static pressure taps on the duct walls to measure fan performance. These rakes were also removed for acoustic measurements. The muffler plug nozzle (fig. 2(a)) was calibrated as a weight flow meter; this application is explained in reference 2. The accuracy of the weight flow measurement is believed to have been about ± 0.5 percent based on use of a standard bellmouth inlet for calibration of the fan weight flow.

PROCEDURE

Detailed explanations of the conditions and procedures used for acquiring inlet aerodynamic performance data (i. e., pressure recovery and distortion) are given in reference 2. Acoustics data were obtained at conditions and with procedures similar to those discussed in references 5, 6, and 11.

Test Conditions

In the general experiment, four parameters were varied: wind tunnel airflow velocity, model fan rotational speed, fan nozzle (muffler exit) area, and inlet angle to the tunnel airflow. Data were obtained at wind tunnel airflow velocities of 0 and 41 meters per second (80 knots). The tunnel airflow case corresponds to the typical aircraft takeoff-and-landing speed chosen for the QCSEE Project (table III). Fixed fan rotational speeds, between 90 and 110 percent of the design corrected speed, were used. Nozzle area was only varied to maintain a fixed operating line (i. e., relation of fan pressure ratio to weight flow). For the tunnel airflow case, inlet angles of 0°, 15°, and 30° were investigated.

Test Procedure

The variables that establish a model operating condition were set in the following sequence: wind tunnel airflow velocity, fan rotational speed, fan weight flow (by adjustment of the nozzle area), and finally inlet flow angle. The weight flow, as determined by calibrating the plug nozzle, was checked by comparing it with an inlet-static-pressure-against-weight-flow calibration previously established in the aerodynamics experiment (ref. 2). With the other variables remaining fixed, acoustics data were obtained at various fan speeds.

While the model operating condition was being set, the sword microphone boom was at a shallow angle (about 20°) to the inlet centerline. The microphone boom angle is always referred to the inlet centerline in this report. Sword microphone angles for which data were obtained are representative of the forward quadrant below the inlet. For an aircraft, this is the region of interest to a ground observer. For zero inlet flow angle, the microphone position was also representative of a sideline measurement. When the model operating condition was set, the microphone boom angle was varied at 2.5° per second to 120°. During this sweep, the sound pressure levels for the 1/3-octave bands containing the first and second harmonics of the blade passage frequency were recorded on-line and also on magnetic tape. While the recording was continued, the boom was rotated back to the 90° position, where the unfiltered microphone signal was recorded on magnetic tape for 1 minute. The boom rotation was then continued, with filtered microphone data recorded, to the 60° position, where the unfiltered signal was again recorded for 1 minute. Rotation was then continued, with filtered on-line data recorded, to the 20° position. Microphone signal filters were then changed to record sound pressure levels for 1/3-octave bands containing frequencies 1.5 and 2.5 times the blade passage frequency (broadband noise). As the boom was swept continuously to 120° and back to 20°, on-line traces for these frequencies were obtained. Data for the ceiling or sideline microphones (fig. 3) were recorded on magnetic tape when the sword microphone boom was at the fixed 60° and 90° positions.

Data Analysis Procedure

Most of the noise data presented herein were recorded on magnetic tape, as previously indicated; and 1/3-octave band analysis was performed later with a standard commercially available analyzer. Model sound pressure level spectra obtained with tunnel airflow were then corrected for background noise. This correction was generally less than 2 decibels and only significant at frequencies near 1000 hertz. Frequencies below 1000 hertz were not considered in the data analysis because, as stated in the section

APPARATUS, the test section is not anechoic below this frequency. Background noise spectra are presented with the results of the experiment.

Data obtained from the fixed microphones in the flyover and sideline planes were extrapolated to realistic aircraft distances and were adjusted to Federal Aviation Regulations - Part 36 (FAR-36) standard conditions of 298 K (537° R) and 70-percent relative humidity by using computerized methods.[1] As previously indicated, the data from the fixed ceiling microphones were extrapolated to a 152-meter (500-ft) sideline. Sword microphone data, obtained with fixed boom angles, were also extrapolated to a 152-meter (500-ft) sideline when the inlet flow angle was zero. For nonzero flow angles, the sword microphone data were extrapolated to a distance of 176 meters (577 ft), which is equivalent to a 152-meter (500-ft) sideline with the boom angle set at 60° to the inlet centerline.

Model acoustics data obtained with the fixed microphones were also adjusted to the size of the QCSEE propulsion system (refs. 1, 9, and 10). The ratio of the QCSEE fan diameter to the model fan diameter is 3.55. Therefore, if the adjustment of sound pressure level (SPL) is based on the ratio of fan areas (i.e., diameter squared), an increment of 11.0 decibels must be added to the model data according to standard logarithmic scaling relations. Model 1/3-octave-band SPL frequencies were adjusted to engine scale by considering the model blade passage frequency and the previously noted fan diameter ratio. For example, for inlet design weight flow, the model fan was operated at a rotational speed that corresponded to a model blade passage frequency of 2155 hertz, which is nearest to the 2000-hertz, 1/3-octave-band center frequency. At engine scale, the blade passage frequency is, therefore, 607 hertz (2155/3.55), which is nearest to the 630-hertz centerband frequency, resulting in a model-to-engine frequency shift of five 1/3-octave bands.

Perceived noise levels were calculated for the scaled and extrapolated microphone data using a computerized procedure based on the requirements of FAR-36.

RESULTS AND DISCUSSION

Fan Aerodynamic Performance

The fan map in figure 5 shows the operating line (pressure ratio against weight flow) used for the acoustic experiment; it was based on the data obtained in the aerodynamics part of the experiment reported in reference 2. As indicated by the relatively low stage

[1]Private communication from F. J. Montegani. Unpublished computer program for band attenuations by numerical integration using pure-tone atmospheric attenuation results from NASA CR-2760. Program available on request.

total pressure ratio, the fan is representative of a very high-bypass-ratio turbofan engine and is typical of those recently considered for application to STOL transport aircraft (ref. 15).

The fan inlet performance for this operating line is shown in figure 6, which gives the average inlet throat Mach number M_{th} as a function of fan speed N for both inlets. This average or one-dimensional Mach number, M_{th}, was determined from the measured fan weight flow and the inlet throat area (corresponding to D_{th} of fig. 4(a)). Deviations from the parabolic representation of the high-Mach-inlet data (fig. 6(b)) are representative of the 0.5-percent accuracy believed applicable to the weight-flow measurement. Deviations for the no-wind-tunnel-airflow case may also have been caused by inflow disturbances related to the large stream tube required to be drawn into the confined test section or by atmospheric disturbances.

Forward Velocity Effects on Inlet Noise

Directional characteristic. - The results presented in this section emphasize the 60° angle from the inlet centerline. A previous experiment (refs. 9 and 10) with the same inlets and a different fan, conducted in an anechoic chamber, suggested that sideline perceived noise had a maximum level near the 60° angle. Reference 16 states that similar results have been noted in other experiments. Procedures for the present experiment were planned, therefore, to emphasize this angle, although sound pressure level spectra were also obtained at 90° from the inlet centerline.

Figure 7 shows model sound pressure levels at the blade passage frequency for both inlets obtained with the sword microphone as the boom rotated from about 20° to 120°. Data are shown as measured on the arc swept by the boom and also as adjusted to a sideline distance of 3.6 fan diameters (i.e., the boom length). The cases shown are representative of the inlet design weight flow with no tunnel airflow but are typical of all other cases. The sideline values, obtained with a standard logarithmic relation based on distance ratio, indicate that the sound pressure levels peaked near 60°, as expected.

Figure 8 shows sound pressure level spectra (at engine scale) obtained for the high-Mach inlet with the sword microphone at fixed boom angles of 60° and 90°. As in figure 7, this case represents the inlet design weight flow with no tunnel airflow. The data, adjusted to the 152-meter (500-ft) sideline, reveal that the SPL was greater at 60° than at 90°, except for the very lowest frequency, where they were about equal. Further examples of directivity are discussed later.

Perceived noise. - Figure 9 shows 152-meter- (500-ft) sideline perceived noise levels scaled to engine size from sword microphone data for both inlets at an angle of 60° from the inlet centerline and for wind tunnel velocities of 0 and 41 meters per

second (80 knots). Perceived noise reduction characteristics for a high-Mach inlet are also shown.

Perceived noise variability with fan speed is shown in figure 9(a). The noise level was significantly reduced for both inlets with tunnel airflow relative to the no-tunnel-airflow case. The same noise data are shown in figure 9(b) as a function of throat Mach number M_{th}. Although the variability with fan speed was quite smooth (i. e., regular) for all cases, the variation of high-Mach-inlet noise with M_{th} was somewhat erratic for the case with no tunnel airflow. This is indicated by deviations, at high M_{th}, from the least-squares parabola relation, which represents the tunnel-airflow case very well. The deviations may have been caused by small errors in weight flow measurement or by unsteadiness of model operation, as previously mentioned in the section Fan Aerodynamic Performance and indicated in figure 6(b). In any case, because of the good agreement for the tunnel-airflow case, the parabolic representation is also believed to well represent the no-tunnel-airflow case for a fixed fan operating line.

The reduction of noise level observed with the low-Mach inlet for increasing fan speed (fig. 9(a)) or throat Mach number (fig. 9(b)) is a fan source noise characteristic, also exhibited by the fan used in the experiment of references 9 and 10. The reduction of low-Mach-inlet noise resulting from tunnel airflow has been discussed in references 5 and 6. A significant amount of the reduction was caused by the cutoff of the tone at the blade passage frequency, as explained in those references.

At low fan speeds or throat Mach numbers, the noise levels for the high-Mach inlet were equal to those of the low-Mach inlet (figs. 9(a) and (b)). However, as fan speed or throat Mach number was increased, the perceived noise from the high-Mach inlet decreased at a much higher rate than that from the low-Mach inlet, revealing the noise reduction characteristic of the high throat Mach numbers. At low fan speeds, the reduction in noise associated with forward velocity was the same for both inlets, about 2 decibels. At high fan speeds, the noise reduction with forward velocity was also about 2 decibels for the low-Mach inlet, but more than 3 decibels for the high-Mach inlet.

The noise reduction characteristics of the high-Mach inlet are abstracted in figure 9(c). For the purpose of this discussion, reduction is defined as the difference between the noise levels of the low- and high-Mach inlets at equal fan speeds. Perceived noise reduction, with and without tunnel airflow, is shown in figure 9(c) as a function of fan speed and also as a function of throat Mach number for the high-Mach inlet. The largest reduction, about 7. 5 decibels, occurred with simulated forward velocity. Forward velocity apparently increased the noise reduction capability of the high-Mach inlet by about 1. 5 decibels at throat Mach numbers of about 0. 8. Although the noise reduction increment is relatively small, the total effect of flight, more than 3 decibels as noted in figures 9(a) and (b), is significant. In particular, these increments are important when related to the stringent noise goals for a propulsion system such as QCSEE (ref. 1).

The somewhat erratic relation between noise reduction and throat Mach number shown in figure 9(c) for the case of no forward velocity was previously discussed in connection with figure 9(b). The parabolic representation of the noise reduction relation with throat Mach number used in figure 9(c) is believed to be accurate because of its good agreement with the forward-velocity case.

Although tunnel airflow has been shown to increase the noise reduction capability of the high-Mach inlet, the magnitude of the effect approaches the accuracy limitation of the instrumentation noted in reference 11, about 2 decibels. However, in reference 11, this uncertainty was based on an adjustment of the low-Mach-inlet data for no tunnel airflow that was made by using very low-frequency noise measurements as a supplemental calibration of the system. The adjustment was somewhat subjective and, therefore, was not used in this study. The result of the reference 11 adjustment was to decrease the differences in level of the low-Mach-inlet noise with and without tunnel airflow. Such adjusted values would increase by 1 to 2 decibels the effect of tunnel airflow on the perceived noise reduction capability of the high-Mach inlet and suggest that the results of figure 9 are at least qualitatively correct and significant. The measured equivalence of noise levels for the low- and high-Mach inlets at the lowest fan speeds and throat Mach numbers does tend to support, however, the data analysis procedure of this report.

Sound pressure level. - One-third-octave-band sound pressure level spectra are shown in figure 10 for both inlets with and without forward velocity and for various fan speeds. Engine-scale SPL data are presented for the 152-meter (500-ft) sideline. A background noise spectrum for the forward-velocity case is also shown to indicate its relation to the inlet-radiated fan noise.

For the low-Mach inlet (fig. 10(a)), the most significant effect of forward velocity on the SPL spectra is the elimination of the tone at the blade passage frequency (BPF). This effect has been discussed in references 5 and 6; and, therefore, it will only be noted here that it is evidence of the wind tunnel's usefulness for simulating the acoustic environment of atmospheric flight. Figure 10(a) also indicates that the SPL at almost all other frequencies was reduced with tunnel airflow. In particular, second and third harmonic (2 BPF and 3 BPF) tones propagated with and without tunnel airflow, but simulated forward velocity reduced the tone level. However, the results of reference 5, which were obtained with a different fan operating line, did indicate some tone and broadband increases of SPL with tunnel airflow. Also, the adjustment of the low-Mach-inlet spectra without tunnel airflow used in reference 11 would, if correct, dominate some of the broadband effects shown in figure 10(a). Therefore, a generalized relation between SPL and tunnel velocity is not apparent.

It can also be seen that the SPL was generally reduced with increasing fan speed. This result is believed to be a fan source characteristic, as previously noted, and was not related to inlet throat Mach number, which for the low-Mach inlet was too low to cause noise reduction.

Sound pressure level spectra for the high-Mach inlet shown in figure 10(b) exhibit characteristics similar to those noted for the low-Mach inlet. However, increasing fan speed and throat Mach number resulted in a greater reduction of SPL at all frequencies for the high-Mach inlet than for the low-Mach inlet. This is most readily apparent for 106-percent fan speed, which corresponds to the inlet design weight flow and is the only common fan speed for both inlets. It appears that the reduction provided by the high-Mach inlet was a broadband phenomenon. (The background noise associated with tunnel airflow was well below even the most suppressed spectrum (fig. 10(b)), except at the lowest frequency of interest.)

Typical high-Mach-inlet noise reduction (difference between the SPL of the low- and high-Mach inlets) spectra are shown in figure 11 with and without forward velocity for 106-percent fan speed. It does not seem possible to characterize the variation of SPL reduction with frequency for either tunnel-airflow case. In particular, no monotonic variation is clearly evident, and large selective reduction of BPF tones does not seem to have occurred. Care must be taken not to compare the levels of these SPL reduction spectra because of the difference in throat Mach number noted on the figure. As previously stated in the discussion of perceived noise (fig. 9), a problem of weight flow measurement, or flow unsteadiness, occurred for the no-forward-velocity case. Unfortunately, the 106-percent fan speed is the only value for which reduction spectra can be defined.

Flow Angle Effects on Inlet Aerodynamic Performance

A complete presentation and discussion of inlet aerodynamic performance data for this experiment is provided in reference 2. However, before flow angle effects on inlet radiated noise are investigated, some aerodynamic performance data will be provided in order to relate the acoustic and aerodynamic performance.

Pressure recovery and distortion. - Figure 12 shows the total pressure recovery at the fan face and the distortion values measured with tunnel airflow for inlet flow angles between 0° and 30°. The pressure recovery used here is an area-averaged parameter and the distortion index DI is defined in the appendix. Data are given for both inlets over a wide range of throat Mach number and were, of course, obtained in the aerodynamics part of the experiment with the inlet rakes described in the section APPARATUS.

Almost no effect of flow angle is discernible for the low-Mach-inlet data (fig. 12(a)), where the effect of throat Mach number (i.e., weight flow) increase is also very small. Larger effects were noted for the high-Mach inlet (fig. 12(b)), but the levels of performance degradation are not severe enough to cause significant concern relative to possible engine aerodynamic performance. As indicated in reference 2, no flow separation was observed for any of the operating conditions considered herein. The small reductions in

pressure recovery resulting from increased throat Mach number were caused by thickened boundary layers at the fan face due to increased diffusion in the inlet. The small increases in distortion index with increasing inlet flow angle were caused by the thickened boundary layer on the windward side of the inlet that resulted from the asymmetric flow. In general, the high values of pressure recovery and low values of distortion for the flow angle range investigated herein are representative of very good inlet performance. However, even these small performance degradations with inlet flow angle may have resulted in noise generation, particularly at the blade passage frequency, as is noted later.

Pressure recovery and distortion performance were also quite good for the no-forward-velocity case (ref. 2), with very nearly the same results as for the zero-flow-angle cases of figure 12. Therefore, the difference in acoustic characteristics previously noted between the wind-tunnel-off and -on cases is probably not directly attributable to the type of average, total pressure performance reported herein. Any change in acoustic performance with tunnel airflow, or forward velocity, is mainly attributable to a reduction of flow unsteadiness (e.g., atmospheric turbulence, which is prevalent at static conditions and reacts with the fan rotor to create noise). A similar effect is expected in actual flight.

Wall static pressure distributions. - Although the inlets were geometrically axisymmetric, the inlet flow fields for nonzero flow angles were asymmetric. The significance of this on the inlet radiated noise is related to the noise reduction mechanism of the high-throat-Mach-number inlet. Although not completely understood, the mechanism relies on supersonic velocities near the inlet cowl walls in the throat region to block the propagation of fan noise through the inlet. Therefore, for a high-Mach axisymmetric inlet at zero flow angle, the flow field and radiated noise field should be axisymmetric; but, as the flow angle is increased, the flow field becomes increasingly asymmetric and can cause the noise field to also become asymmetric.

Figures 13 and 14 present wall static pressure distributions for the inlets at the design weight flow. The ratio of local wall static pressure to free-stream total pressure is shown as a function of inlet length for flow angles of 0°, 15°, and 30°. Two circumferential positions ψ were considered: 0°, which was the windward side or leading edge of the inlet at nonzero flow angles; and 200° from the windward side. The axisymmetric character of the flow fields at zero inlet flow angle ($\alpha = 0^{\circ}$) is shown by the similarity of the pressure distributions for the two circumferential locations.

Figure 13 illustrates that as inlet flow angle was increased, the low-Mach-inlet wall static pressures at the upstream end of the inlet decreased on the windward side ($\psi = 0^{\circ}$) and increased on the opposite side ($\psi = 200^{\circ}$). No supersonic flow occurred in these flow fields, as indicated by all the static pressures being greater than the value corresponding to Mach 1. However, the static pressures on the windward side do approach the Mach 1

value with increased flow angle; and, therefore, some refraction of noise might be expected in this region.

Figure 14 shows that the high-Mach-inlet wall static pressures varied in the same manner as for the low-Mach inlet. However, some supersonic flow existed at all flow angles on the windward side, with the extent of supersonic flow increasing with increasing flow angle. On the opposite side ($\psi = 200^{\circ}$) of the high-Mach inlet, supersonic flow was noted only at zero flow angle. Therefore, with such a strongly asymmetric flow field, including both supersonic and subsonic regions, refraction of noise and noise field variations with flow angle are certainly to be expected.

Flow Angle Effects on Inlet Noise

Although the variations of inlet noise with forward velocity were regular and easy to characterize, the variations with inlet flow angle were seemingly irregular and difficult to characterize. An obvious reason for this occurrence is the complicated aerodynamic flow field that existed at elevated inlet flow angles, as previously demonstrated. However, another reason might be that the noise variations observed were generally small, about 1 or 2 decibels in perceived noise. Even though the accuracy of the experiment is considered quite good (±0.5 percent for weight flow, ±0.5 dB for sound pressure level), the complex variations of noise with flow angle were small enough to make generalizations difficult.

Perceived noise. - The inlet flow angle effects on perceived noise level are shown in figures 15 and 16. Because of possible directivity variations, the engine-scale results obtained with the sword microphone are shown for fixed boom angles of 60° and 90°. With elevated inlet flow angle, the plane swept by the microphone boom was representative of an aircraft flyover plane with the observer (i.e., the microphone) below the aircraft.

Figure 15 shows the variation of perceived noise with fan speed at fixed inlet flow angles of 0°, 15°, and 30°. The results are presented in this manner because, as explained in the section PROCEDURE, this is the manner in which the model data were obtained. The low-Mach-inlet noise variation with flow angle was between 0.2 and 3 decibels. At 60° from the low-Mach-inlet centerline (fig. 15(a)), no regular variation is apparent. The variation with flow angle is different at each fan speed. At 106-percent fan speed, the noise level for the 15° flow angle appears to be an anomaly; but because of the complex flow and noise fields, this is not certain. At 90° from the low-Mach-inlet centerline (fig. 15(b)), the variation of noise with flow angle appears more regular (e.g., peak noise at the 15° flow angle), but the variation was significantly larger at 96-percent fan speed than at 106- or 110-percent fan speed.

Some similarities in the high-Mach-inlet noise levels with flow angle can be noted. The 15° and 30° flow angle noise levels were generally no more than 1 decibel apart for both the 60° location (fig. 15(a)) and the 90° location (fig. 15(b)). The noise levels for zero flow angle showed more variation, being somewhat higher than for the other flow angles at all speeds, except 110 percent where they were about equal or lower. At the high-Mach-inlet design weight flow (106-percent fan speed), the variation of noise level with flow angle was less than 2 decibels (figs. 15(a) and (b)). The largest variation of noise level with flow angle for the high-Mach inlet occurred at 103-percent fan speed and was only slightly greater than 2 decibels (fig. 15(a)).

Figure 16 presents the same results as figure 15 with inlet throat Mach number replacing fan speed. Both the 60° and 90° microphone locations were again considered, and the same type of complex variation resulted.

The amount of noise reduction achieved by the high-Mach inlet relative to the low-Mach inlet is shown in figure 17 at the three inlet flow angles for 106-percent fan speed. This information, which was abstracted from the data of figures 15 and 16, again shows the seeming irregularity of the noise level with varying flow angle. Inlet noise was reduced for each flow angle at the two microphone locations. However, the variation is different at the two locations. The greatest variation, slightly more than 2 decibels, was observed at the 60° microphone location between flow angles of 15° and 30°. These results do infer that noise directivity varies with inlet flow angle.

Sound pressure level. - A more complete example of the directivity of the inlet radiated noise at the three inlet flow angles is given in figure 18, where filtered 1/3-octave-band model sound pressure levels are shown for both inlets at the design weight flow condition.

As previously discussed for the perceived noise levels, these SPL data generally show only small variations with inlet flow angle, with no particular regularity. However, the low-Mach-inlet data at twice the blade passage frequency (2 BPF) are quite unique. The lobed directivity for this frequency was previously noted in references 5 and 6 and is discussed in detail in reference 6. At the same fan operating condition, the high-Mach-inlet radiated noise at 2 BPF had a different directional characteristic. The high-throat-Mach-number inlet apparently altered the lobed SPL pattern of the low-Mach inlet, and there is only slight evidence of the lobed characteristic.

Because of the important effect of the 2 BPF tone on the perceived noise, the lobed directivity characteristic of the low-Mach inlet did affect the variation of noise reduction with inlet flow angle shown in figure 17. In particular, comparing figures 17 and 18 shows that, at 60° from the inlet centerline, the largest noise reduction and near maximum sound pressure level at 2 BPF for the low-Mach inlet occurred near the 30° flow angle.

Complete low-Mach inlet, 1/3-octave SPL spectra for fixed boom angles of 60° and 90° are shown in figure 19. Engine-scale results for 106-percent fan speed are

presented for the three inlet flow angles. As previously shown in figure 18, the 2 BPF tone was considerably higher for the 30° flow angle (about 8 dB) than for the lower flow angles at the 60° boom angle (fig. 19(a)) but was greatly reduced for the 90° boom angle (fig. 19(b)). For both microphone locations the low-frequency SPL generally increased with increasing inlet flow angle. At 60° from the inlet centerline, the tone at the blade passage frequency, which was effectively cut off at zero inlet flow angle, became evident as flow angle was increased. However, at the 30° flow angle, the tone was only about 2.5 decibels higher than at zero flow angle. At 90° from the inlet centerline, the tone was not apparent for any flow angle. Occurrence of the tone at nonzero flow angles may be evidence of a flow distortion effect on noise. For high frequencies (greater than 2 BPF), SPL generally decreased with increasing flow angle at the 60° boom angle and was relatively invariant at the 90° boom angle.

Sound pressure level (SPL) and reduction spectra for the high-Mach inlet are given in figure 20 for the two microphone locations. Except for the tone at the blade passage frequency, no regular variation of SPL with flow angle at low frequencies is apparent. The BPF tone, cut off at zero flow angle, became evident as flow angle was increased, being about 3.5 decibels higher at 30° than at 0° flow angle for both microphone locations. For high frequencies (greater than 2 BPF), there was some evidence of a small decrease in SPL between 0° and 15° flow angles (fig. 20) at both microphone locations. However, because the SPL levels in this region were generally lower than levels at harmonics, particularly the 2 BPF tone, no large effect on perceived noise was incurred.

The prominent feature of the reduction spectra shown in figure 20 is the relatively large reduction at twice the blade passage frequency indicated at the 30° inlet flow angle for the 60° boom angle. This occurrence and its absence at the 90° boom angle are, of course, related to the lobed directivity pattern for the low-Mach inlet at 2 BPF, which was effectively eliminated by the high-Mach inlet, as previously discussed. For the 60° microphone location, the relatively high reduction at 3 BPF can also be related to a significant harmonic tone for the low-Mach inlet, indicated in figure 19(a). No large broadband effect of frequency on noise reduction is clearly evident for either microphone location.

Simulated In-Flight Inlet Noise at a Ground Sideline Station

As mentioned in the previous section, the noise measurements obtained with the sword microphone with the inlets at nonzero flow angles were representative of an aircraft flyover plane. Acoustic measurements for a representative sideline plane with the model at a simulated altitude were obtained with microphones installed in the test section ceiling (fig. 3). These microphones were arranged to simulate the sideline location chosen for the QCSEE Project (ref. 1); the aircraft takeoff flight characteristics are

given in table III. A schematic representation of the in-flight simulation is shown in figure 21, which defines the sideline acoustic observer position 60 meters (200 ft) below and 152 meters (500 ft) to the side of the aircraft in a takeoff configuration. The inlet upwash angle shown in figure 21 is equivalent to the inlet flow angle of the isolated-nacelle experiment discussed herein. The three ceiling microphones (fig. 3) represent observer angles (fig. 21) of 60°, 75°, and 90°.

Engine-scale perceived noise levels obtained with these microphones for both inlets operated at the design weight flow condition (106-percent fan speed) are shown in figure 22. As in the case of the flyover plane, the maximum noise level was observed at the 60° observer angle. The high-Mach-inlet noise levels were about 7 decibels lower than the low-Mach-inlet noise levels at each observer angle, which is similar to the noise reductions obtained with the sword microphone (figs. 9(c) and 17) with tunnel airflow.

Figure 23 presents the 1/3-octave sound pressure level spectra for both inlets and a reduction spectrum at the 60° sideline station for the design weight flow condition. A background noise level is also shown and indicates interference only at the very lowest frequency of interest, where the data have been corrected for its effect. The spectra for the inlet radiated noise are similar to those shown in figure 10 for the forward-velocity case and obtained with the sword microphone at a fixed boom angle. The noise reduction spectrum for the simulated in-flight case for nonzero altitude and inlet flow angle (fig. 23) is similar in level to that previously shown in figure 11 for zero flow angle with the observer on a 152-meter (500-ft) sideline and at the same altitude as the engine or aircraft. The level is also similar to those shown in figure 20 for an observer in a flyover plane at a nonzero inlet flow angle. However, a small gradual increase of SPL reduction with frequency, not evident in figures 11 and 20, is evident in figure 23.

SUMMARY OF RESULTS

An experiment was conducted to determine the effects of simulated flight on the acoustic characteristics of a high-throat-Mach-number fan inlet. The noise reduction capability of the inlet, which was operated to throat Mach numbers of about 0.8, was determined by comparing its performance with that of a conventional low-throat-Mach-number (about 0.6) inlet at anechoic wind tunnel air velocities of 0 and 41 meters per second (80 knots), and inlet flow angles up to 30°. A representative 50.8-centimeter (20-in.) diameter, low-pressure-ratio model fan was used as the noise source. The primary results of the experiment were as follows:

1. Simulated forward velocity caused perceived noise level reductions of about 2 decibels for the low-throat-Mach-number inlet at all fan speeds or throat Mach numbers. For the high-throat-Mach-number inlet, the noise reduction with tunnel airflow varied

from 2 decibels to more than 3 decibels with increasing fan speed and throat Mach number.

2. High-throat-Mach-number-inlet perceived noise reduction, defined as the difference between noise levels of the two inlets for the same fan operating condition, was as high as 7.5 decibels with tunnel airflow and about 6 decibels without tunnel airflow.

3. Aerodynamic performance measurements disclosed high fan inlet pressure recovery and low distortion for all inlet flow angles. For nonzero flow angles, wall static pressure measurements suggested strongly asymmetric flow fields in the upstream region of the inlets. This is believed to have caused refraction of radiated noise and directivity variations with flow angle, particularly for the high-throat-Mach-number inlet, which had a complex combination of subsonic and supersonic flows in this region.

4. Effects of inlet flow angle on perceived noise were seemingly irregular and difficult to characterize because of the complex noise and flow fields and generally small noise variations. At the inlet design weight flow condition, the perceived noise from the high-throat-Mach-number inlet varied less than 2 decibels with inlet flow angles up to 30°, with the highest noise level at 0° and the lowest at 15°.

5. One-third-octave-band sound pressure level spectra showed that without tunnel airflow the tone at the blade passage frequency propagated but that with tunnel airflow and zero inlet flow angle the tone was cut off (i.e., did not propagate) for all fan speeds investigated. Tunnel airflow also resulted in lower sound pressure levels at almost all other frequencies of interest. Reappearance of the blade passage tone for nonzero flow angles (as much as 3.5 dB relative to the zero-flow-angle case) revealed a possible effect of the small inlet flow distortion.

6. The high-throat-Mach-number inlet effectively eliminated a multilobe directivity pattern observed at twice the blade passage frequency for the low-throat-Mach-number inlet at nonzero flow angles.

Lewis Research Center,
National Aeronautics and Space Administration,
Cleveland, Ohio, August 17, 1977,
738-01.

APPENDIX - SYMBOLS

a	ellipse semi-major axis of internal inlet lip (fig. 4)
b	ellipse semi-minor axis of internal inlet lip (fig. 4)
c	external forebody length (fig. 4)
D	diameter
DI	inlet total pressure distortion index, (Maximum total pressure - Minimum total pressure)/Average total pressure
d	external forebody thickness
f	frequency
L	length
M	Mach number
N	fan speed, percent of design rotational speed
P	total pressure
p	static pressure
V	velocity
W	weight flow
x	axial distance from inlet highlight (fig. 4)
y	radial distance from inlet highlight (fig. 4)
α	inlet flow angle (fig. 4)
δ	ratio of total pressure to standard sea-level pressure
θ	ratio of total temperature to standard sea-level temperature
λ_{max}	maximum diffuser wall angle (fig. 4)
ψ	inlet circumferential position (fig. 4)

Subscripts:

c	centerbody
d	diffuser
e	exit
hl	inlet highlight
HM	high-throat-Mach-number inlet
LM	low-throat-Mach-number inlet

max	maximum
th	inlet throat
0	free stream
2	fan face or rake measuring plane
3	fan stage exit

REFERENCES

1. Ciepluch, Carl C.: A Review of the QCSEE Program. NASA TM X-71818, 1975.
2. Abbott, John M.; Diedrich, James H.; and Williams, Robert C.: Low Speed Aerodynamic Performance of 50.8-Centimeter-Diameter Noise Suppressing Inlets for the Quiet, Clean, Short-Haul Experimental Engine (QCSEE). NASA TP-1178, 1978.
3. Diedrich, James H.; and Luidens, Roger W.: Measurement of Model Propulsion System Noise in a Low-Speed Wind Tunnel. AIAA Paper 76-91, Jan. 1976.
4. Rentz, Peter E.: Softwall Acoustical Characteristics and Measurement Capabilities of the NASA Lewis 9 × 15 Foot Low Speed Wind Tunnel. (BBN-3176, Bolt, Beranek, and Newman, Inc.; NASA Contract NAS3-19410.) NASA CR-135026, 1976.
5. Dietrich, D. A.; Heidmann, M. F.; and Abbott, J. M.: Acoustic Signatures of a Model Fan in the NASA-Lewis Anechoic Wind Tunnel. AIAA Paper 77-59, Jan. 1977.
6. Heidmann, M. F.; and Dietrich. D. A.: Simulation of Flight-Type Engine Fan Noise in the NASA-Lewis 9 × 15 Anechoic Wind Tunnel. NASA TM X-73540, 1976.
7. Hickcox, T. E.; et al.: Low-Speed and Angle-of-Attack Effects on Sonic and Near-Sonic Inlets. (D6-42392, Boeing Commercial Airplane Co.; NASA Contract NAS3-18035.) NASA CR-134778, 1975.
8. Miller, Brent A.; Dastoli, Benjamin J.; and Wesoky, Howard L.: Effect of Entry-Lip Design on Aerodynamics and Acoustics of High-Throat-Mach-Number Inlets for the Quiet, Clean, Short-Haul Experimental Engine. NASA TM X-3222, 1975.
9. Bilwakesh, K. R.; and Clemons, A.: Acoustic Tests on a 20-Inch (50.8 cm) Diameter Scale Model (1 : 3.5) Fan and Inlet for the Under-the-Wing Engine, Vol. I. NASA CR-135117, 1977.
10. Bilwakesh, K. R.; and Clemons, A.: Acoustic Tests on a 20-Inch (50.8 cm) Diameter Scale Model (1 : 3.5) Fan and Inlet for the Under-the-Wing Engine, Vol. II. NASA CR-135118, 1977.
11. Heidmann, M. F.; and Dietrich, D. A.: Effects of Simulated Flight on Fan Noise Suppression. AIAA Paper 77-1334, Oct. 1977.
12. Yuska, J. A.; Diedrich, James H.; and Clough, Nestor: Lewis 9- by 15-Foot V/STOL Wind Tunnel. NASA TM X-2305, 1971.

13. Lewis, George W., Jr.; and Tysl, Edward R.: Overall and Blade-Element Performance of a 1.20-Pressure-Ratio Fan Stage at Design Blade Setting Angle. NASA TM X-3101, 1974.

14. Wasserbauer, Charles A.: Calculated Performance Map of a $4\frac{1}{2}$-Stage 15.0-Centimeter- (5.9-In.-) Mean-Diameter Turbine Designed for a Turbofan Simulator. NASA TM X-2822, 1973.

15. Luidens, Roger W.; et al.: Engine Noise Technology. STOL Technology. NASA SP-320, 1972, pp. 371-412.

16. Saule, Arthur V.: Modal Structure Inferred From Static Far-Field Noise Directivity. NASA TM X-71909, 1976.

TABLE I. - MODEL FAN CHARACTERISTICS

Diameter, cm (in.)	50.8 (20.0)
Number of rotor blades	15
Number of stator vanes	25
Vane-blade ratio	1.67
Rotor-stator spacing, true rotor tip chords	1
Hub-tip radius ratio	0.46
Rotor tip solidity	0.91
Rotor hub solidity	1.20
Design corrected tip speed, m/sec (ft/sec)	213 (700)
Design corrected fan speed, rpm (percent)	8020 (100)
Design blade passage frequency, BPF, Hz	2005
Design and operating blade angle, deg	0

TABLE II. - SUMMARY OF INLET GEOMETRIC VARIABLES

(a) Internal lip

Geometric variable	Low-Mach inlet	High-Mach inlet
Contraction ratio, $(D_{hl}/D_{th})^2$	1.46	1.46
Surface contour	Ellipse	Ellipse
Proportions, a/b	2.0	2.0

(b) External forebody

Diameter ratio, D_{hl}/D_{max}	0.880	0.900
Ratio of length to maximum diameter, c/D_{max}	0.310	0.219
Surface contour[a]	DAC-1	DAC-1
Proportions, c/d	5.166	4.380

(c) Diffuser

Ratio of exit flow area to inlet flow area, $\left(D_e^2 - D_c^2\right)/D_{th}^2$	1.011	1.156
Ratio of diffuser length to exit diameter, L_d/D_e	0.850	0.856
Maximum local wall angle, λ_{max}, deg	8.7	8.7
Location of maximum local wall angle, percent L_d	33.8	50
Equivalent conical half-angle, deg	0.17	2.08
Surface contour	Cubic	Cubic

(d) Centerbody

Ratio of length to diameter, L_c/D_c	0.935	0.935
Surface contour	NACA-1	NACA-1
Ratio of centerbody length to diffuser length, L_c/L_d	0.416	0.418
Ratio of centerbody diameter to diffuser exit diameter, D_c/D_e	0.46	0.46

(e) Overall

Ratio of inlet length to diffuser exit diameter, L/D_e	1.035	1.029

[a]The DAC-1 contour was developed by the Douglas Aircraft Company and is given by

$$\left(\frac{y}{d}\right)^2 = 2.318\left(\frac{x}{c}\right) - 2.748\left(\frac{x}{c}\right)^2 + 2.544\left(\frac{x}{c}\right)^3 - 1.113\left(\frac{x}{c}\right)^4$$

TABLE III. - QCSEE PROJECT AIRCRAFT TAKEOFF

FLIGHT CHARACTERISTICS FOR

ACOUSTIC CALCULATIONS

Aircraft speed, m/sec (knots)	41.15 (80)
Aircraft climb angle to horizon, deg	12.5
Wing angle of attack, deg	6
Inlet upwash angle, deg	15
Angle between inlet centerline and wing chord, deg	5
Altitude, m (ft)	61 (200)
Sideline distance, m (ft)	152 (500)

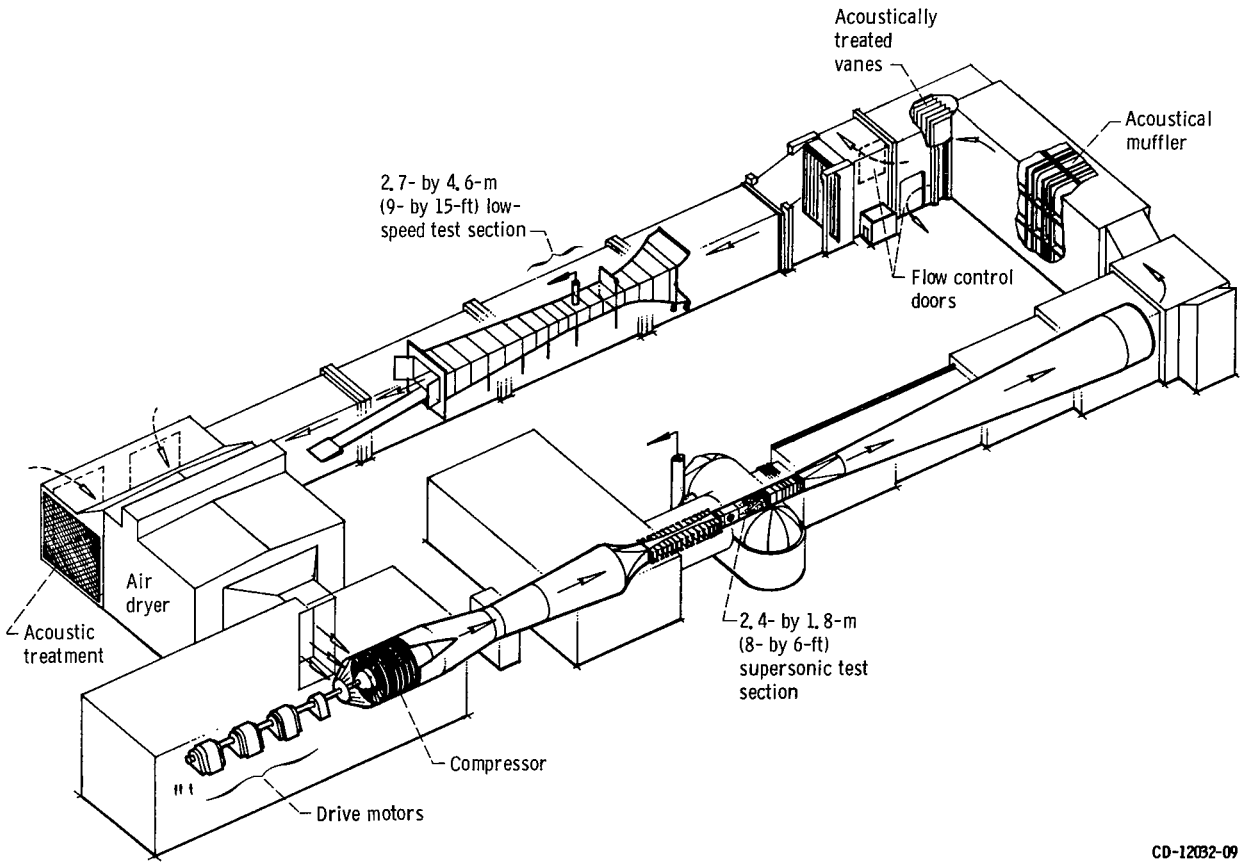

Figure 1. - NASA Lewis 8- by 6-Foot Wind Tunnel and 9- by 15-Foot V/STOL Wind Tunnel.

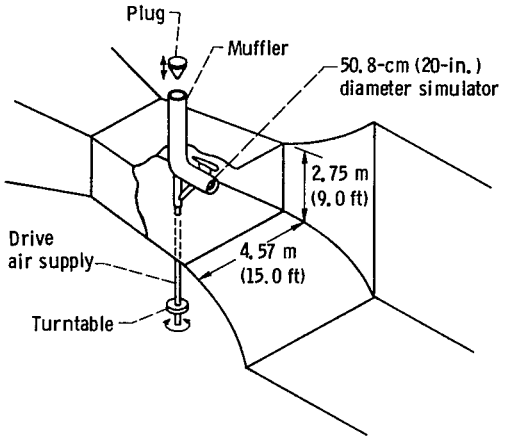

(a) Arrangement of model in test section.

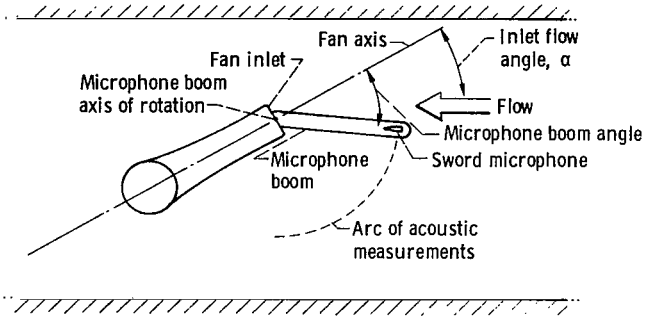

(b) Plan view.

Figure 2. - Schematic views of 9- by 15-Foot V/STOL Wind Tunnel showing model installation.

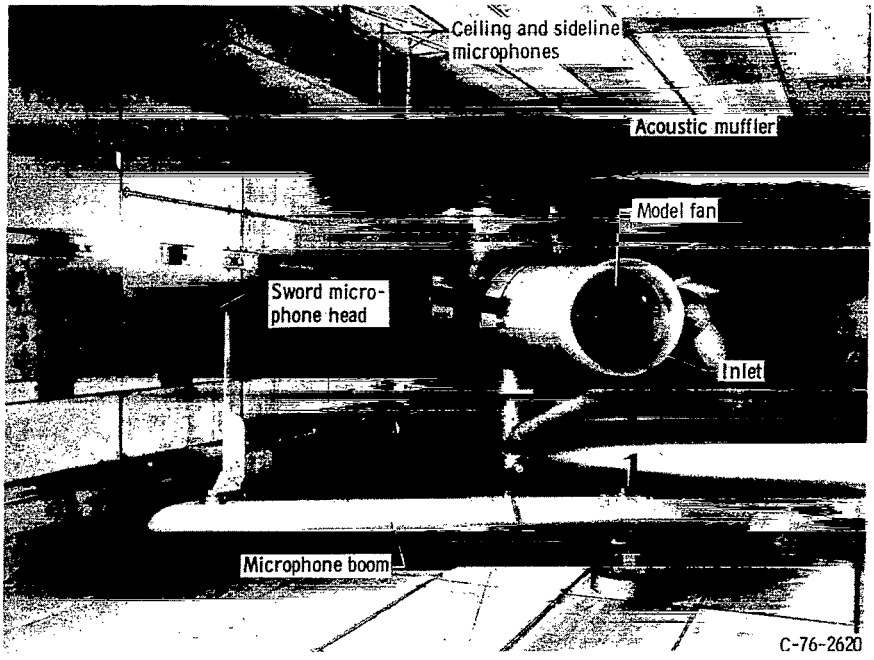

Figure 3. - Fan engine model installed in anechoic wind tunnel, looking downstream.

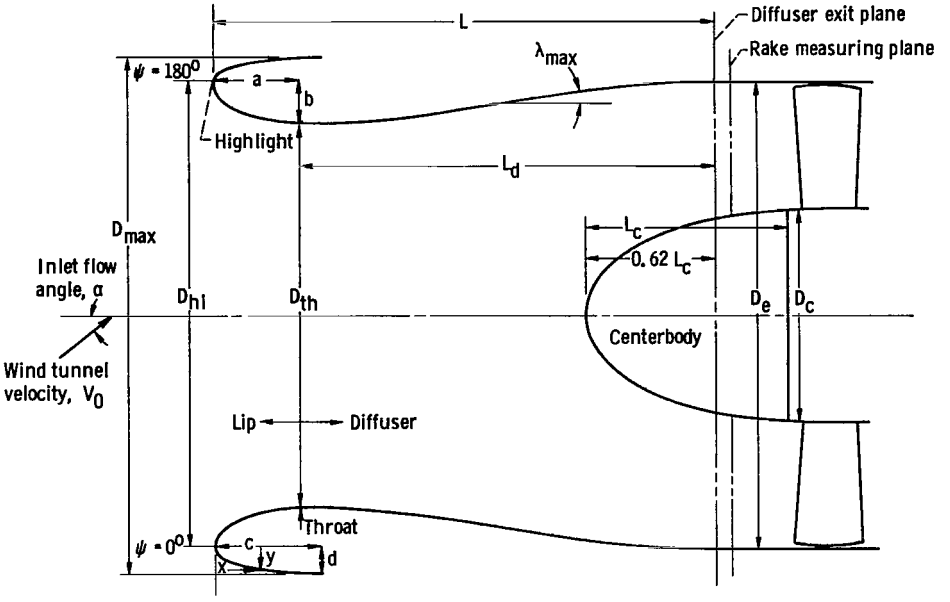

(a) Inlet nomenclature.

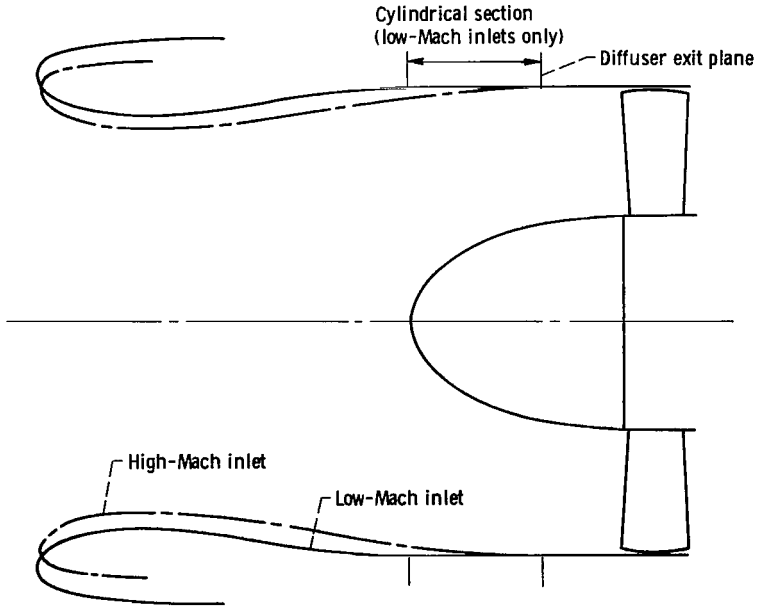

(b) Comparison of inlets.

Figure 4. - Inlet designs.

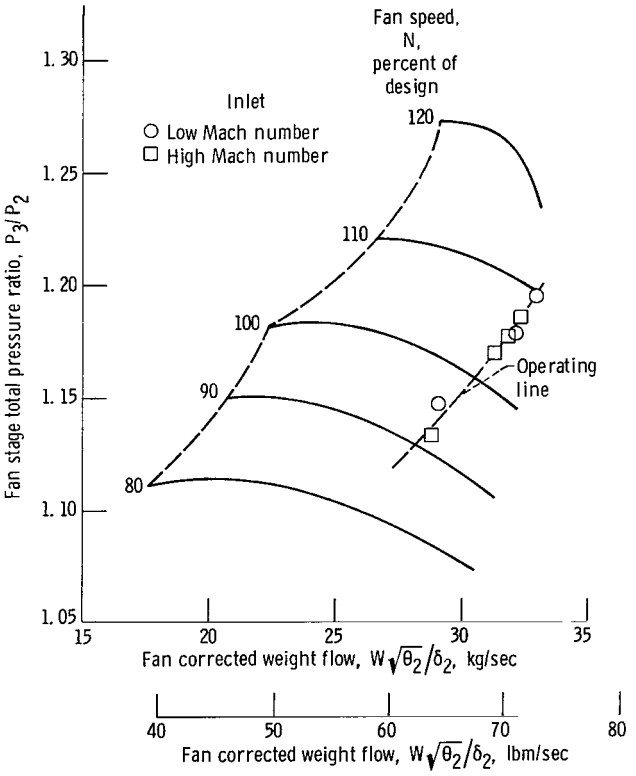

Figure 5. - Model fan performance.

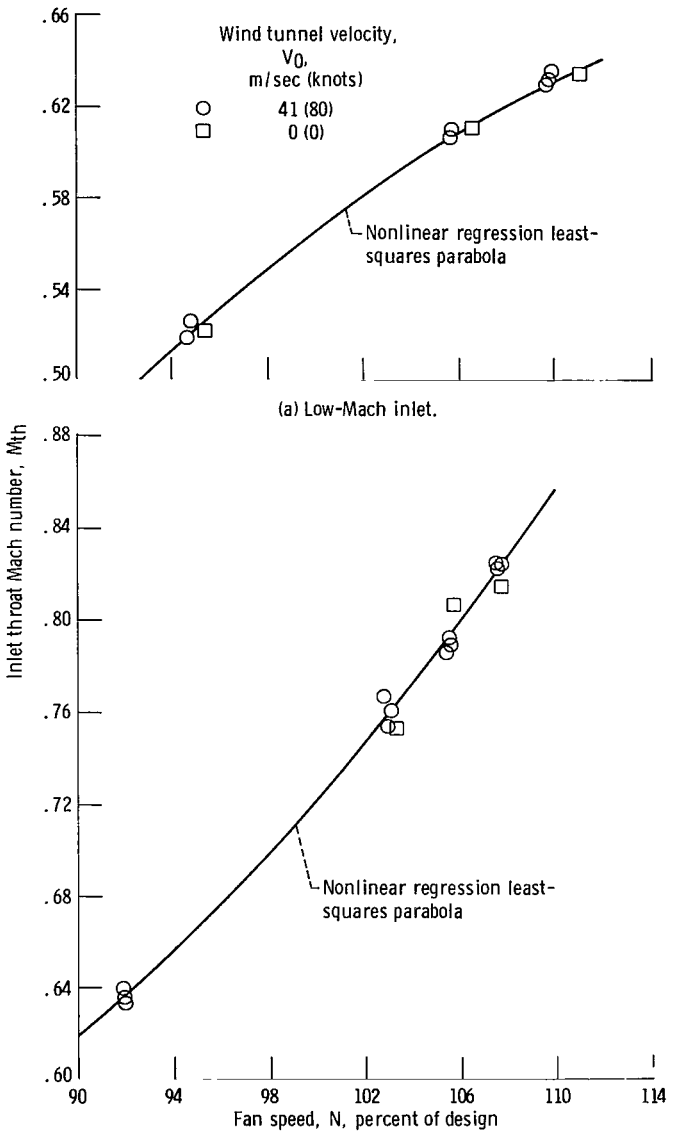

Figure 6. - Effect of fan speed on inlet throat Mach number.

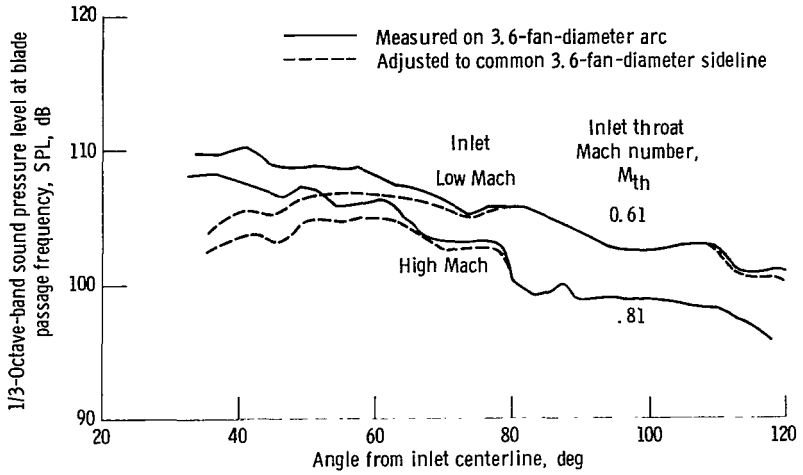

Figure 7. - Effect of noise direction on blade passage tone. Scale, model; wind tunnel velocity, V_0, 0; fan speed, N, 106 percent of design.

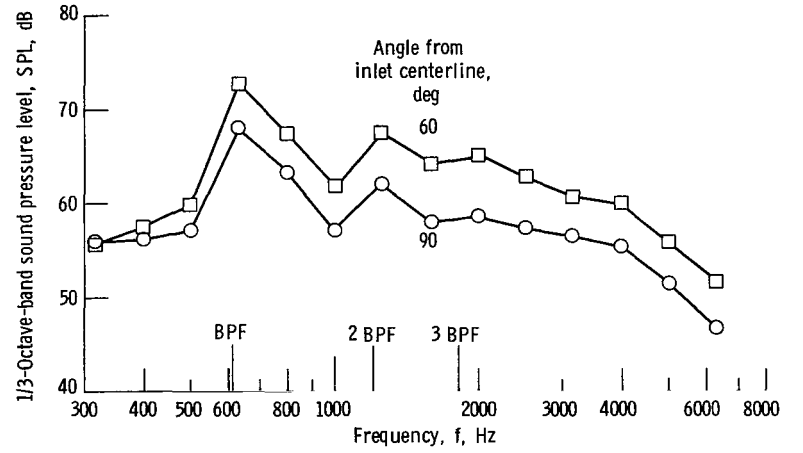

Figure 8. - Effect of noise direction on sound pressure level for high-Mach inlet. Scale, engine; wind tunnel velocity, V_0, 0; fan speed, N, 106 percent of design; throat Mach number, M_{th}, 0.81; observer location, 152-meter (500-ft) sideline; ambient temperature, 298 K (537^0 R); relative humidity, 70 percent.

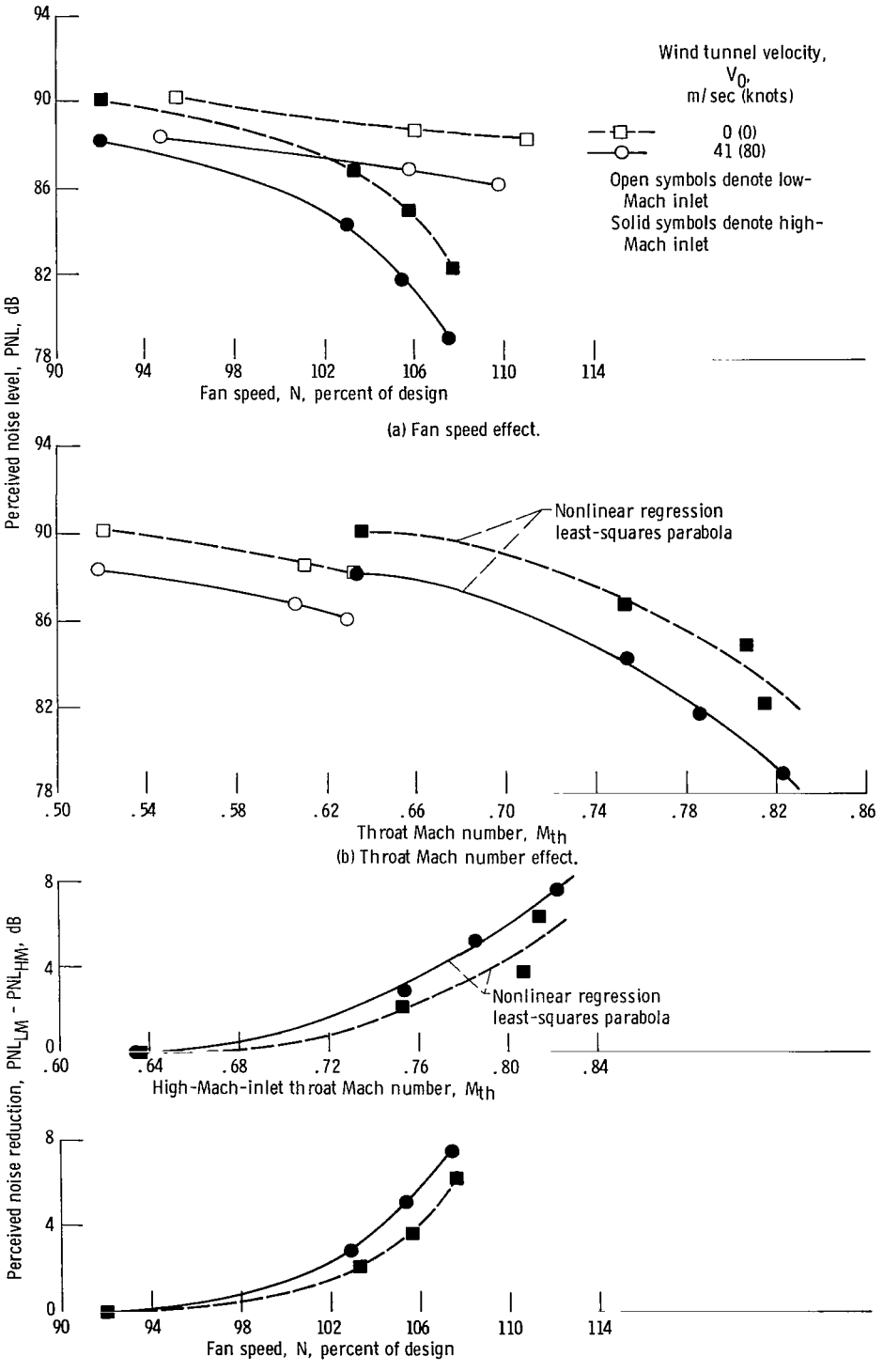

Figure 9. - Effect of forward velocity on perceived noise. Scale, engine; inlet flow angle, α, 0^0; observer location, 152-meter (500-ft) sideline; boom angle, 60^0 from inlet centerline; ambient temperature, 298 K (537^0 R); relative humidity, 70 percent.

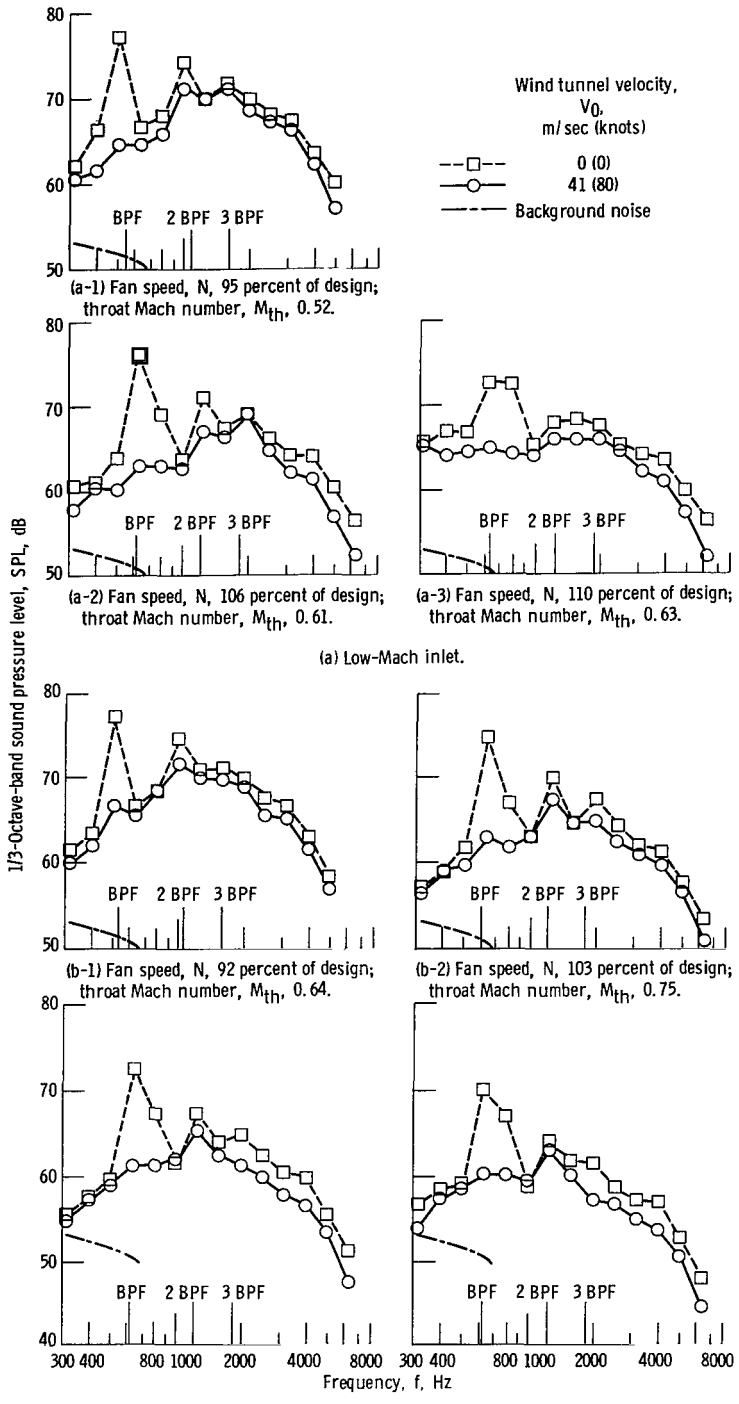

(a-1) Fan speed, N, 95 percent of design; throat Mach number, M_{th}, 0.52.

(a-2) Fan speed, N, 106 percent of design; throat Mach number, M_{th}, 0.61.

(a-3) Fan speed, N, 110 percent of design; throat Mach number, M_{th}, 0.63.

(a) Low-Mach inlet.

(b-1) Fan speed, N, 92 percent of design; throat Mach number, M_{th}, 0.64.

(b-2) Fan speed, N, 103 percent of design; throat Mach number, M_{th}, 0.75.

(b-3) Fan speed, N, 106 percent of design; throat Mach number, M_{th}, 0.80.

(b-4) Fan speed, N, 108 percent of design; throat Mach number, M_{th}, 0.82.

(b) High-Mach inlet.

Figure 10. - Effects of fan speed and forward velocity on sound pressure level. Scale, engine; inlet flow angle, α, 0^0; observer location, 152-meter (500-ft) sideline; boom angle, 60^0 from inlet centerline; ambient temperature, 298 K (537^0 R); relative humidity, 70 percent.

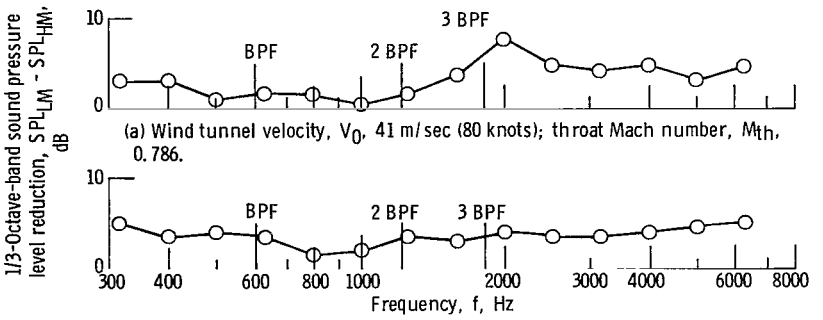

(a) Wind tunnel velocity, V_0, 41 m/sec (80 knots); throat Mach number, M_{th}, 0.786.

(b) Wind tunnel velocity, V_0, 0; throat Mach number, M_{th}, 0.807.

Figure 11. - Typical high-Mach-inlet noise reduction spectra. Scale, engine; fan speed, N, 106 percent of design; inlet flow angle, α, 0^0; observer location, 152-meter (500-ft) sideline; boom angle, 60^0 from inlet centerline; ambient temperature, 298 K (537^0 R); relative humidity, 70 percent.

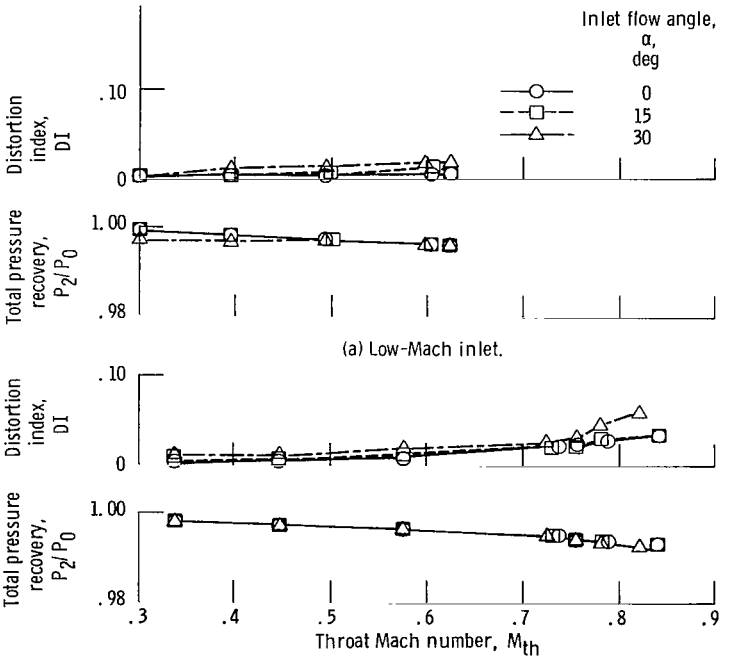

(a) Low-Mach inlet.

(b) High-Mach inlet.

Figure 12. - Effect of throat Mach number on inlet pressure recovery and distortion. Wind tunnel velocity, V_0, 41 m/sec (80 knots).

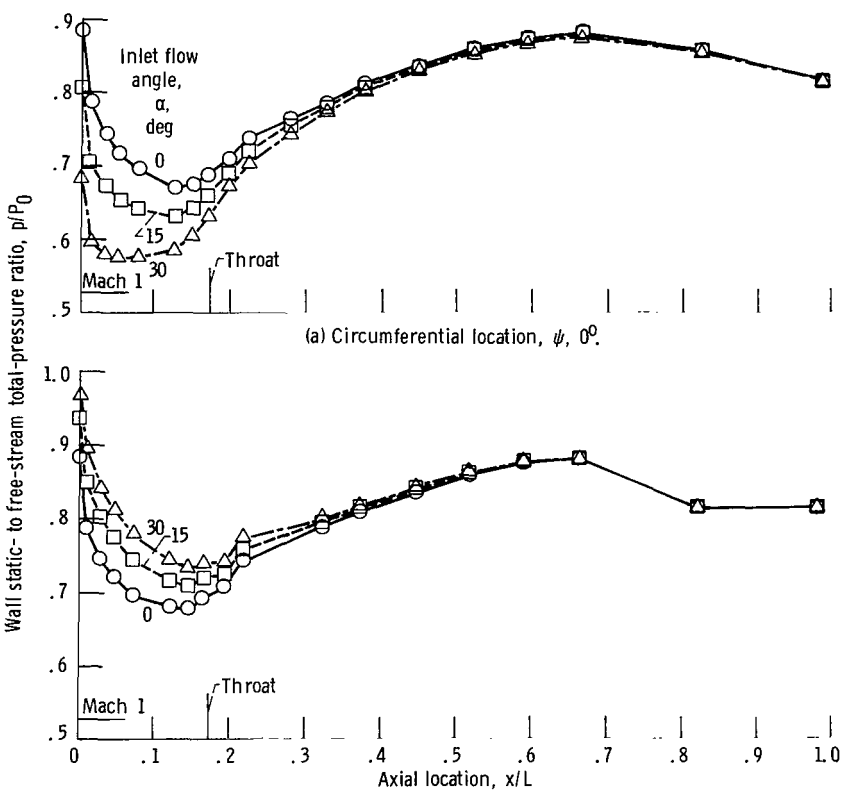

Figure 13. - Low-Mach-inlet wall static pressure distribution. Wind tunnel velocity, V_0, 41 m/sec (80 knots); fan speed, N, 106 percent of design; throat Mach number, M_{th}, 0.61.

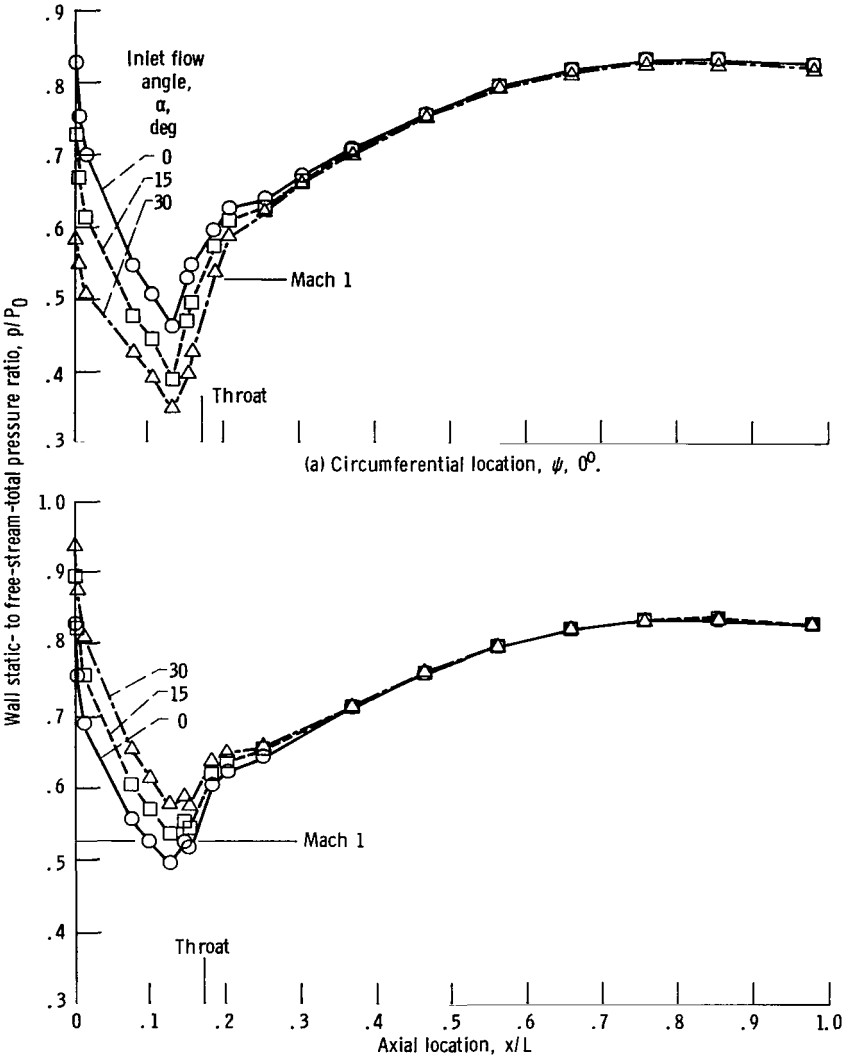

Figure 14. - High-Mach-inlet wall static pressure distribution. Wind tunnel velocity, V_0, 41 m/sec (80 knots); fan speed, N, 106 percent; throat Mach number, M_{th}, 0.79.

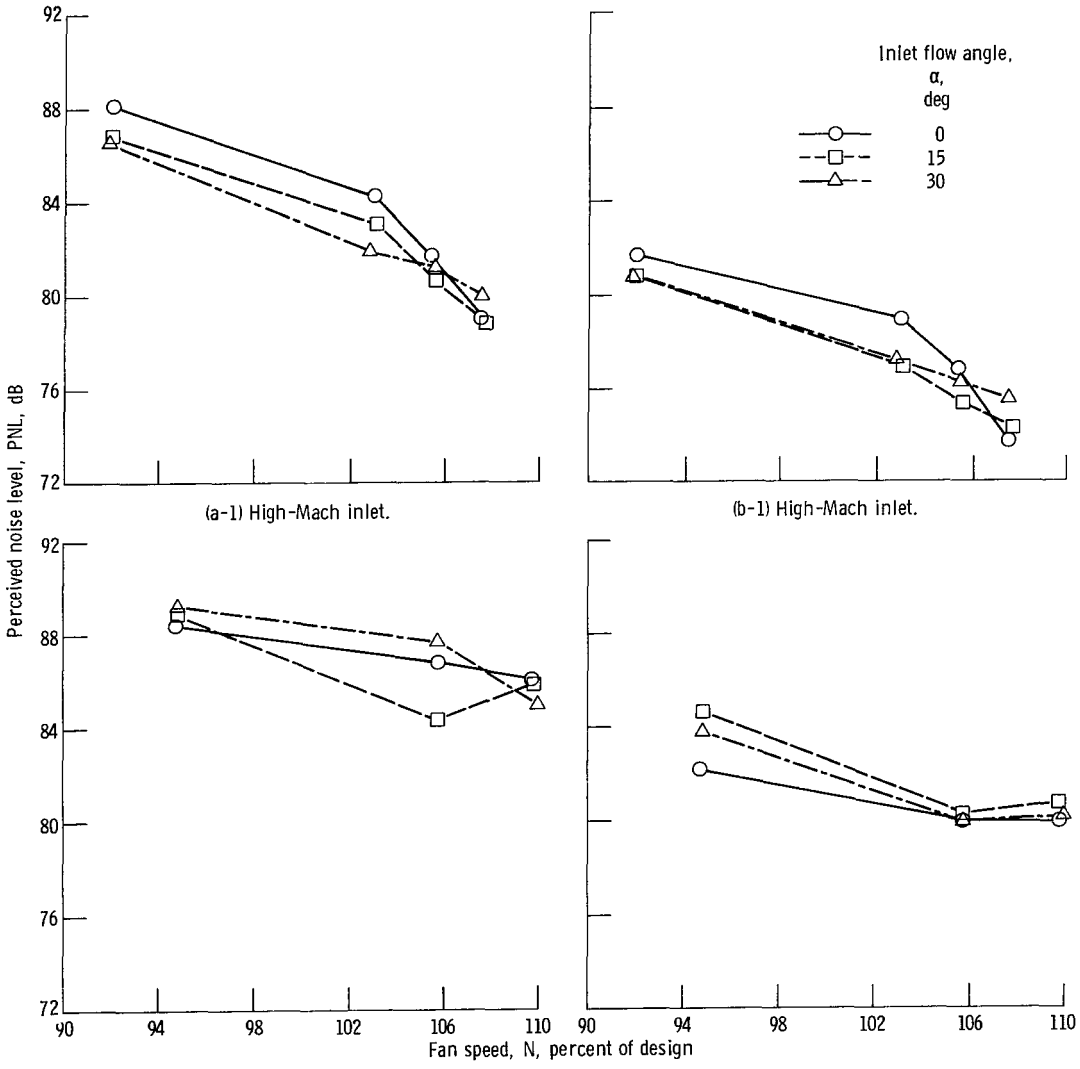

Figure 15. - Effect of inlet flow angle on perceived noise level, as function of fan speed. Scale, engine; wind tunnel velocity, V_0, 41 m/sec (80 knots); observer location, 176-meter (577-ft) arc; ambient temperature, 298 K (537° R); relative humidity, 70 percent.

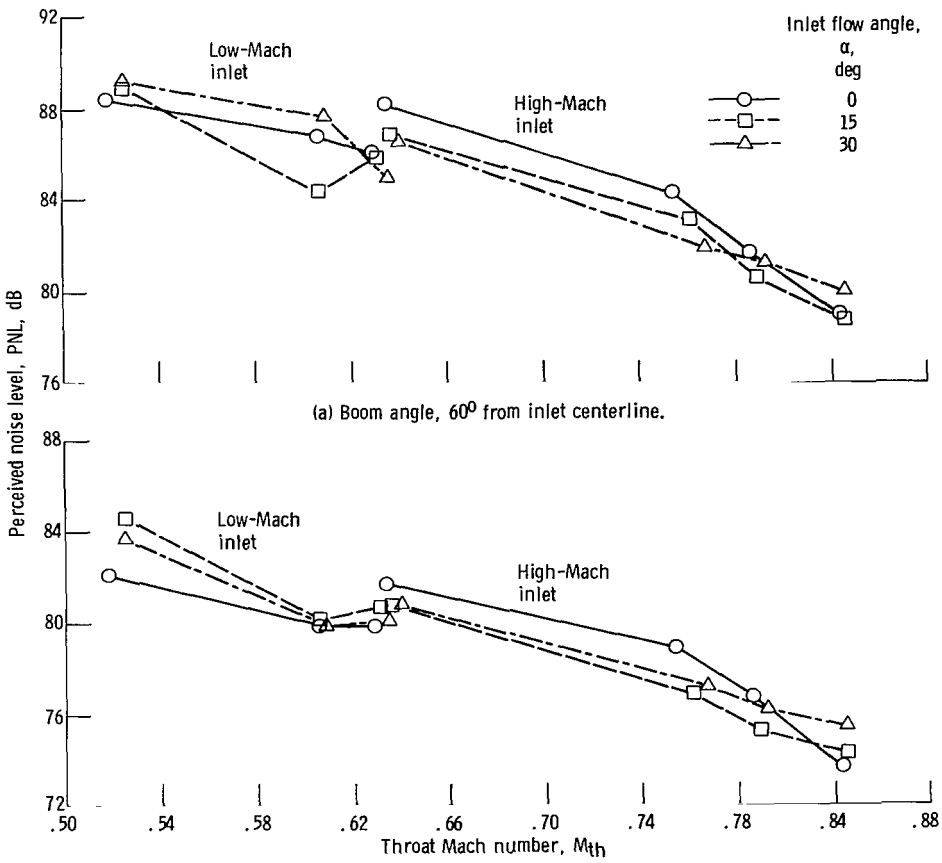

(a) Boom angle, 60^0 from inlet centerline.

(b) Boom angle, 90^0 from inlet centerline.

Figure 16. - Effect of inlet flow angle on perceived noise, as function of throat Mach number. Scale, engine; wind tunnel velocity, V_0, 41 m/sec (80 knots); observer location, 176-meter (577-ft) arc; ambient temperature, 298 K (537^0 R); relative humidity, 70 percent.

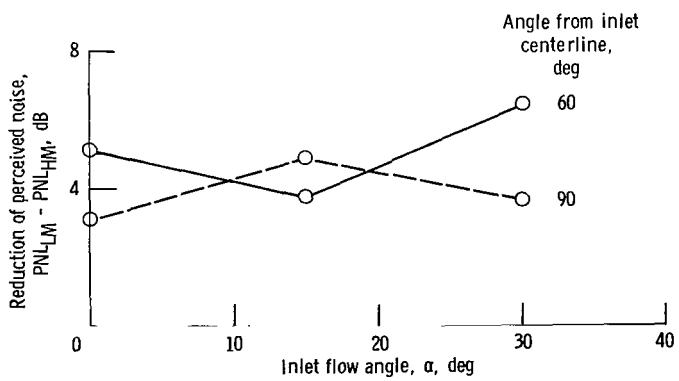

Figure 17. - Effect of inlet flow angle on perceived noise reduction for high-Mach inlet. Scale, engine; wind tunnel velocity, V_0, 41 m/sec (80 knots); fan speed, N, 106 percent of design; observer location, 176-meter (577-ft) arc; ambient temperature, 298 K (537^0 R); relative humidity, 70 percent.

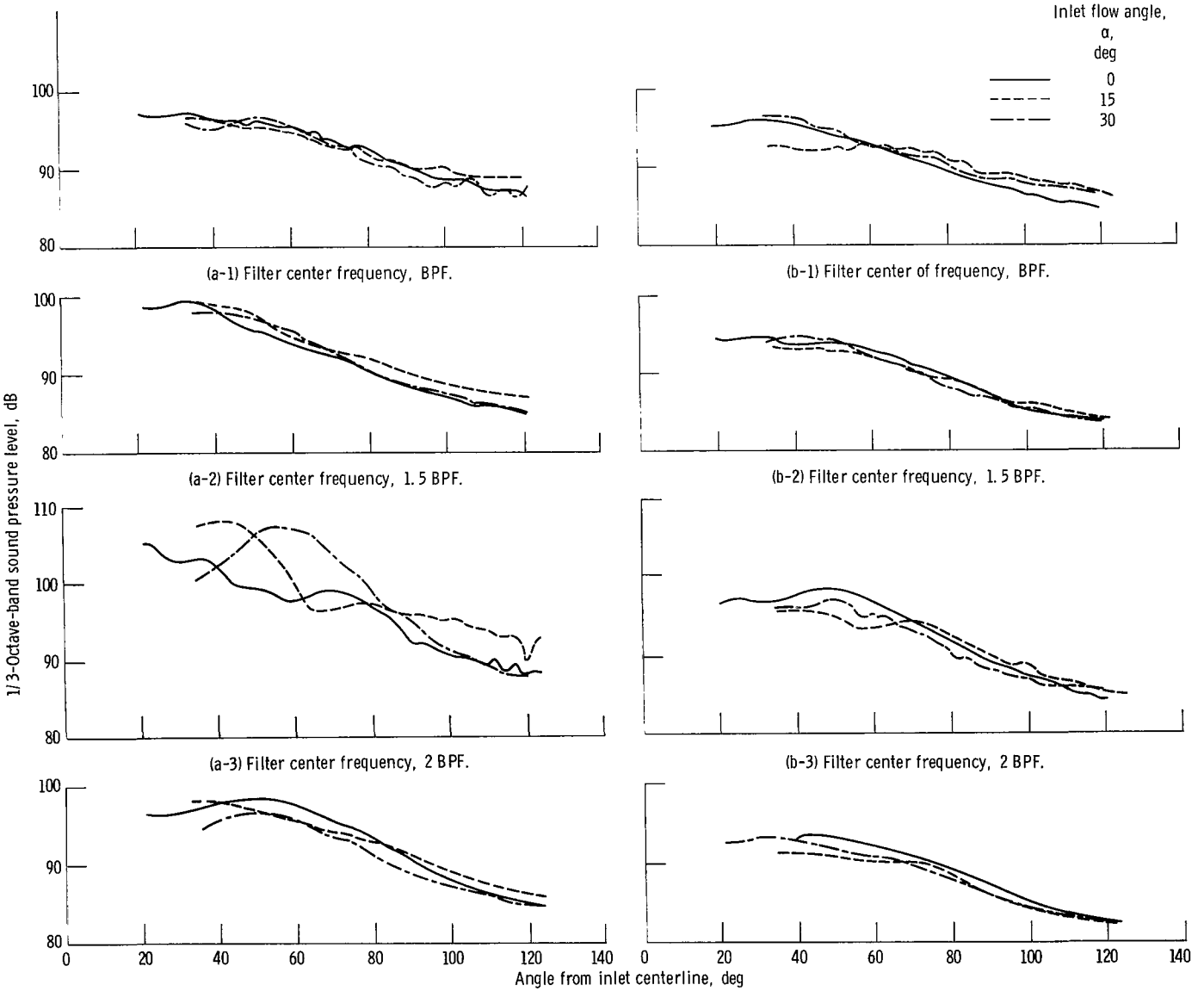

(a) Low-Mach inlet; throat Mach number, M_{th}, 0.61.

(b) High-Mach inlet; throat Mach number, M_{th}, 0.79.

Figure 18. - Effect of inlet flow angle on model noise directivity. Wind tunnel velocity, V_0, 41 m/sec (80 knots); fan speed, N, 106 percent of design.

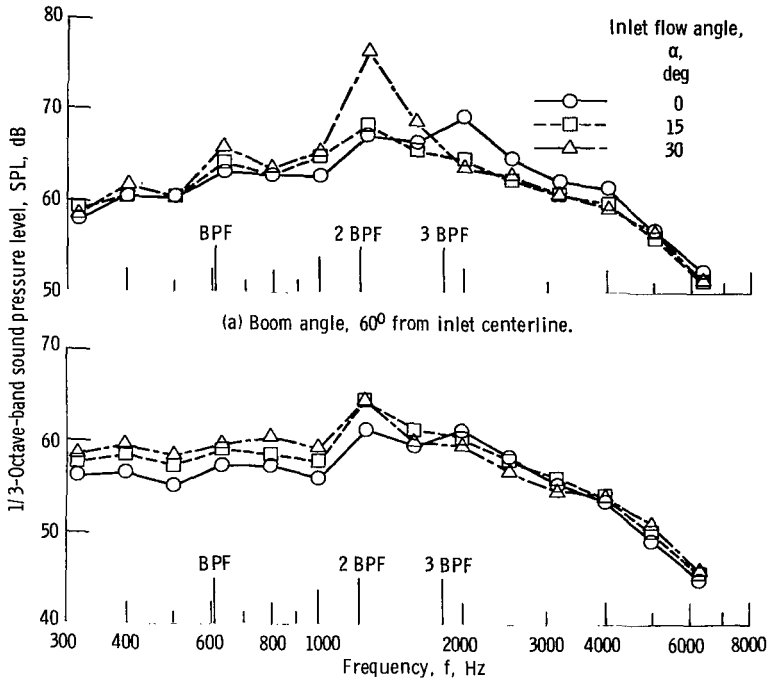

(a) Boom angle, 60° from inlet centerline.

(b) Boom angle, 90° from inlet centerline.

Figure 19. - Effect of inlet flow angle on sound pressure level for low-Mach inlet. Scale, engine; wind tunnel velocity, V_0, 41 m/sec (80 knots); fan speed, N, 106 percent of design; throat Mach number, M_{th}, 0.61; observer location, 176-meter (577-ft) arc; ambient temperature, 298 K (537° R); relative humidity, 70 percent.

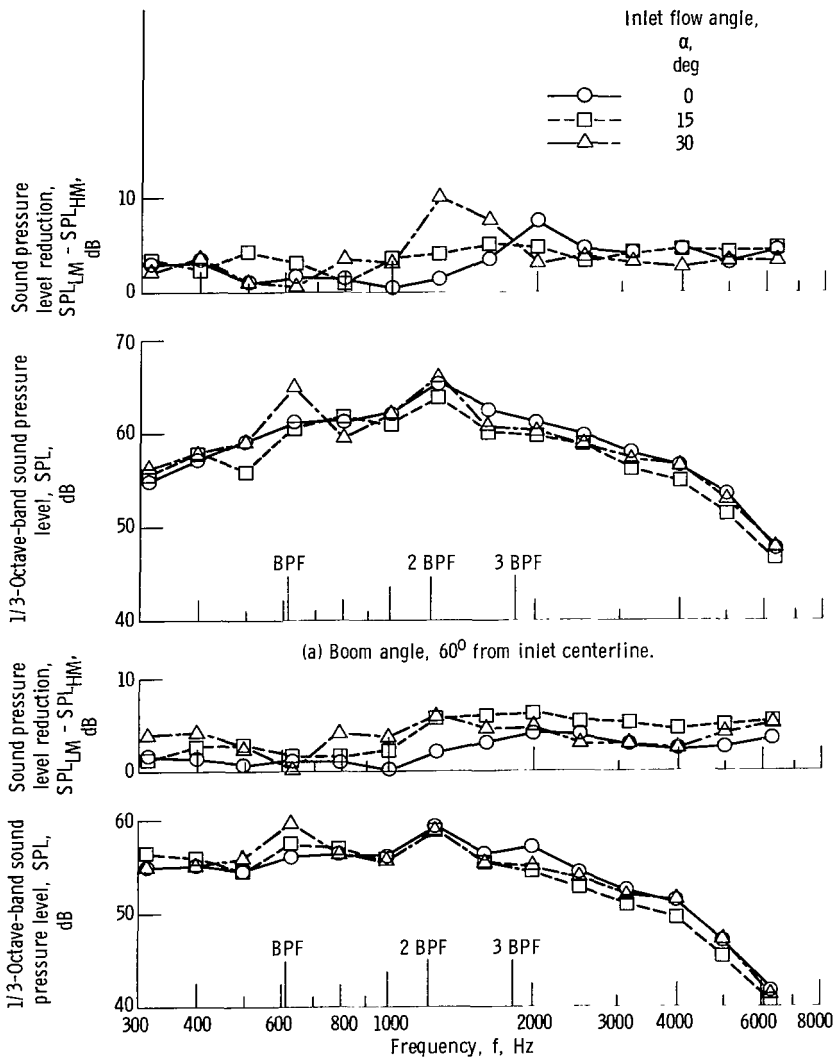

(a) Boom angle, 60^{o} from inlet centerline.

(b) Boom angle, 90^{o} from inlet centerline.

Figure 20. - Effect of inlet flow angle on sound pressure level for high-Mach inlet. Scale, engine; wind tunnel velocity, V_0, 41 m/sec (80 knots); fan speed, N, 106 percent of design; throat Mach number, M_{th}, 0.79; observer location, 176-meter (577-ft) arc; ambient temperature, 298 K (537^{o} R); relative humidity, 70 percent.

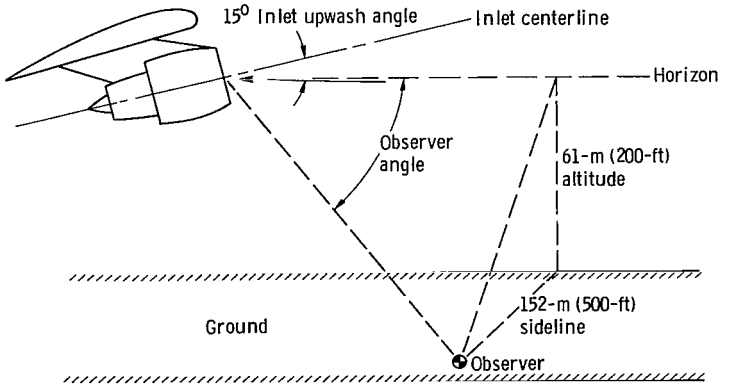

Figure 21. - Definition of sideline acoustic observer position simulated by test section ceiling microphones.

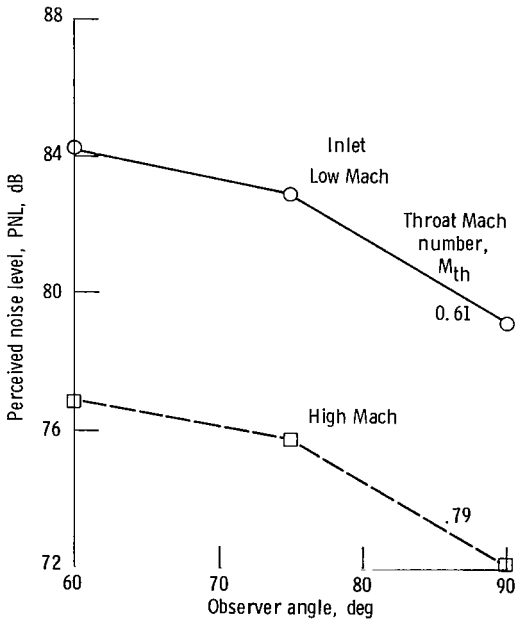

Figure 22. - Simulated in-flight perceived noise at ground sideline station. Scale, engine; wind tunnel velocity, V_0, 41 m/sec (80 knots); fan speed, N, 106 percent of design; inlet flow angle, α, 15°; observer location, 152-meter (500-ft) sideline; altitude, 61 meters (200 ft); ambient temperature, 298 K (537° R); relative humidity, 70 percent.

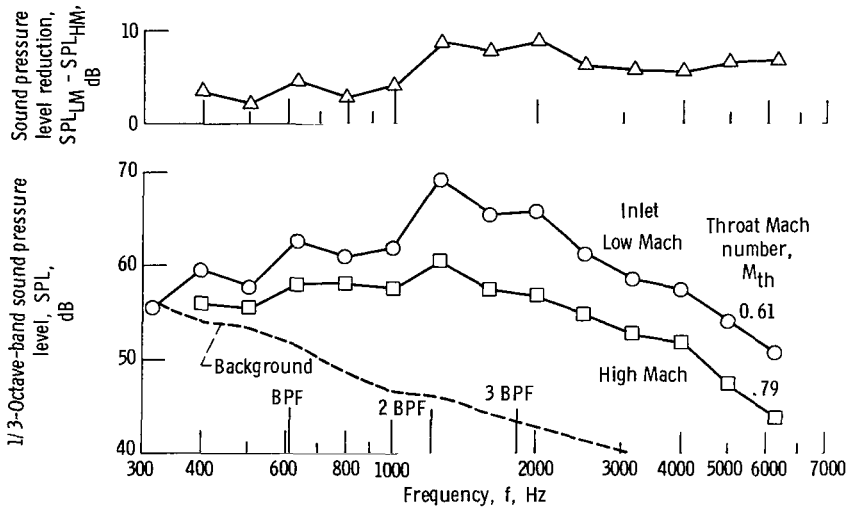

Figure 23. - Simulated in-flight sound pressure level at 60^0 ground sideline station. Scale, engine; wind tunnel velocity, V_0, 41 m/sec (80 knots); fan speed, N, 106 percent of design; inlet flow angle, α, 15^0; observer location, 152-meter (500-ft) sideline; altitude, 61 meters (200 ft); ambient temperature, 298 K (537^0 R); relative humidity, 70 percent.

1. Report No.	2. Government Accession No.	3. Recipient's Catalog No.
NASA TP-1199		

4. Title and Subtitle	5. Report Date
SIMULATED FLIGHT EFFECTS ON NOISE CHARACTERISTICS OF A FAN INLET WITH HIGH THROAT MACH NUMBER	April 1978
	6. Performing Organization Code
7. Author(s)	8. Performing Organization Report No.
Howard L. Wesoky, Donald A. Dietrich, and John M. Abbott	E-9253
	10. Work Unit No.
9. Performing Organization Name and Address	738-01
National Aeronautics and Space Administration Lewis Research Center Cleveland, Ohio 44135	11. Contract or Grant No.
	13. Type of Report and Period Covered
12. Sponsoring Agency Name and Address	Technical Paper
National Aeronautics and Space Administration Washington, D.C. 20546	14. Sponsoring Agency Code

15. Supplementary Notes

16. Abstract

An anechoic wind tunnel experiment was conducted to determine the effects of simulated flight on the noise characteristics of a high-throat-Mach-number (about 0.8) fan inlet. Comparisons were made with the performance of a conventional low-throat-Mach-number (about 0.6) inlet with the same 50.8-cm (20-in.) fan noise source. Simulated forward velocity of 41 m/sec (80 knots) reduced perceived noise levels for both inlets, the largest effect being more than 3 dB for the high-throat-Mach-number inlet. The high-throat-Mach-number inlet was as much as 7.5 dB quieter than the low-throat-Mach-number inlet with tunnel airflow and about 6 dB quieter without tunnel airflow. Effects of inlet flow angles up to 30° were seemingly irregular and difficult to characterize because of the complex flow fields and generally small noise variations (about 2 dB for perceived noise). Some modifications of tones and directivity at blade passage harmonics resulting from inlet flow angle variation were noted.

17. Key Words (Suggested by Author(s))	18. Distribution Statement
High throat Mach number inlet Fan noise Inlet noise	Unclassified - unlimited STAR Category 07

19. Security Classif. (of this report)	20. Security Classif. (of this page)	21. No. of Pages	22. Price*
Unclassified	Unclassified	43	A03

* For sale by the National Technical Information Service, Springfield, Virginia 22161

NASA-Langley, 1978

National Aeronautics and Space Administration

Washington, D.C.
20546

Official Business
Penalty for Private Use, $300

THIRD-CLASS BULK RATE

Postage and Fees Paid
National Aeronautics and
Space Administration
NASA-451

5 1 1U,A, 032778 S00903DS
DEPT OF THE AIR FORCE
AF WEAPONS LABORATORY
ATTN: TECHNICAL LIBRARY (SUL)
KIRTLAND AFB NM 87117

NASA

POSTMASTER: If Undeliverable (Section 158, Postal Manual) Do Not Return